Check for updates

Accepted Article

Duvalo "Volcano" (North Macedonia): A Purely Tectonic-related CO_2 Degassing System

L. Li Vigni[1-2], C. Cardellini[3], M. Temovski[4], A. Ionescu[3-5], K. Molnár[4], L. Palcsu[4], A. L. Gagliano[2], S. Cappuzzo[2], and W. D'Alessandro[2]

[1]Dipartimento di Scienze della Terra e del Mare, Università di Palermo, Italy.

[2]Istituto Nazionale di Geofisica e Vulcanologia (INGV) – Sezione di Palermo, Italy.

[3]Dipartimento di Fisica e Geologia, Università di Perugia, Italy.

[4]Isotope Climatology and Environmental Research Centre, Institute for Nuclear Research, Debrecen, Hungary.

[5]ISUMADECIP, Faculty of Environmental Science and Engineering, Babes-Bolyai University, Cluj-Napoca, Romania.

Corresponding author: Walter D'Alessandro (walter.dalessandro@ingv.it)

Key Points:

- The total CO_2 output from Duvalo "volcano" has been estimated for the first time
- Gas compositions rule out significant mantle contributions or recent volcanic activity while geothermal activity is improbable
- An active fault system favors indirect gas production and upflow to the Earth's surface.

This article has been accepted for publication and undergone full peer review but has not been through the copyediting, typesetting, pagination and proofreading process, which may lead to differences between this version and the Version of Record. Please cite this article as doi: 10.1029/2021GC010198.

This article is protected by copyright. All rights reserved.

Abstract

Duvalo "volcano" is a site of anomalous geogenic degassing close to Ohrid (North Macedonia) not related to volcanic activity, despite its name. CO_2 flux measurements made with the accumulation chamber (321 sites over ~50,000 m^2) showed fluxes up to nearly 60,000 g m^{-2} d^{-1}, sustaining a total output of ~67 t d^{-1}. Soil gas samples were taken at 50 cm depth from sites with high CO_2 fluxes and analyzed for their chemical and isotope composition. The gas is mainly composed by CO_2 (> 90%) with significant concentrations of H_2S (up to 0.55 %) and CH_4 (up to 0.32 %). The isotope compositions of He (R/R_A 0.10) and of CO_2 ($\delta^{13}C$ ~0‰) exclude significant mantle contribution, while $\delta^{13}C$-CH_4 (~ -35‰) and $\delta^{2}H$-CH_4 (~ -170‰) suggest a thermogenic origin for CH_4. The area is characterized by intense seismic activity and Duvalo corresponds to an active tectonic structure bordering the Ohrid graben. The production of H_2S within the stratigraphic sequence may be explained by thermochemical reduction of sulfate. The uprising H_2S is partially oxidized to sulfuric acid that, reacting with carbonate rocks, releases CO_2. The tectonic structure of the area favors fluid circulation, sustaining H_2S production and oxidation, CO_2 production and allowing the escape of the gases to the atmosphere. In the end, Duvalo represents a tectonic-related CO_2 degassing area whose gases originate mostly, if not exclusively, in the shallowest part of the crust (<10 km). This finding highlights that even systems with trivial mantle contribution may sustain intense CO_2 degassing (> 1000 t km^{-2} d^{-1}).

Plain Language Summary

The carbon cycle is an important piece of the puzzle of the present climate change. While anthropogenic sources of atmospheric carbon are reasonably constrained, geological sources are much less. Among the latter, carbon release to the atmosphere in seismically active areas, though known from decades, is less studied. Here we estimate the total emission of carbon dioxide from Duvalo, an area near Ohrid (North Macedonia). The obtained value (67 metric tons per day) is comparable with some active volcanic areas in the region. Although local inhabitants call this area Duvalo volcano, no recent volcanic activity is recognized here. The composition of the gas released by this system seems also to rule out geothermal activity or deep contributions from the Earth's mantle. This study shows that natural degassing systems with relatively shallow crustal sources (few kilometers), may sustain intense gas emissions from the soil.

1 Introduction

During the last decades there has been great interest in the scientific community in estimating the degassing flux of carbon from the Earth's interior to the atmosphere. Among the greenhouse gases, carbon dioxide and methane are considered to be the most effective species contributing to the global warming. In 2011, the global abundance of CO_2 and CH_4 was, respectively, 391 ppm and 1,803 ppb (IPCC, 2014), but still increasing. The observations for 2018 reported in the fifteenth WMO Greenhouse Gas Bulletin show a global mean abundance of CO_2 and CH_4 respectively of 407.8 ± 0.1 ppm and 1,869 ± 2 ppb. They represent the main contributors to the total amount of geogenic carbon degassing to the atmosphere, playing a crucial role in the global carbon cycle (Delmelle & Stix, 1999). Despite a significant improvement in the worldwide dataset, the global flux of CO_2 degassing from the Earth's interior is still the least well-quantified part of the global cycle (Berner & Lasaga, 1989). On geological time scales, the evolution of atmospheric CO_2 levels and Earth climate was mainly controlled by the competing effect of deeply-derived CO_2 flux into the atmosphere and the atmospheric CO_2 sink by chemical weathering (Kerrick & Caldeira, 1993)

This article is protected by copyright. All rights reserved.

Accepted Article

Many studies have been devoted to the quantification of the release of deeply-derived CO_2 to the atmosphere from different geological settings (e.g., Brune et al., 2017; Kerrick, 2001; Mörner & Etiope, 2002) and most of them have focused on the present-day CO_2 emission from volcanoes (Brantley & Koepenick, 1995; Burton et al., 2013; Fischer & Aiuppa, 2020; Fischer et al., 2019; Le Guern, 1982; Werner et al., 2019). However, the close relationship between tectonically active areas and geogenic carbon emissions has long been evidenced (Barnes et al., 1978; Irwin & Barnes, 1980) and several authors have attempted to estimate non-volcanic degassing, which contributes a globally-significant amount of geogenic CO_2 (Frondini et al., 2019; Chiodini et al., 1999; 2000; 2011; Kerrick et al., 1995; Lewicki & Brantley, 2000; Seward & Kerrick, 1996; Tamburello et al., 2018; Yuçe et al., 2017). According to Barnes et al. (1978) and Irwin and Barnes (1980), the main tectonic degassing areas are located along geodynamically active regions. Fault zones play an important role in CO_2 transfer by creating preferential pathways for gas-carrying fluid transport from the deep crust or the mantle to the Earth's surface (Faulkner et al., 2010; Hunt et al., 2017; Muirhead et al., 2016), escaping through the soil into the atmosphere as result of pressure decrease (King, 1986). At a global scale, the geographical distribution and the amount of deeply-derived CO_2 are controlled by regional normal/transcurrent faulting (Tamburello et al., 2018) and continental rift lengths (Brune et al., 2017).

Carbon dioxide discharges and the main active fault systems are widespread in the Balkan Peninsula. However, the estimation of geogenic CO_2 release from this area is still poorly quantified, and a first regional quantification has been attempted only for Greece (Daskalopoulou et al., 2019).

The Duvalo area is located close to the village of Kosel, in the Ohrid region, in the south-western part of the Republic of North Macedonia (Fig. 1a,b). The natural phenomenon of intense soil degassing (in Macedonian, Duvalo literally means a place where it blows; a blowhole), is responsible for intense soil alteration (Fig. 1c), that has damaged vegetation over a large area (many thousands of m^2), and the deposition of elemental sulfur and sulfate minerals. Between the 16^{th} and 19^{th} centuries, during the Ottoman Empire, Duvalo was mined for sulfur, producing about 1700 kg a^{-1} that was transported to the gunpowder magazines in Thessaloniki, now in Greece, and Istanbul in Turkey (Šerif, 2001). In 1979, the City Council of Ohrid Municipality declared the Duvalo site a natural rarity with unique features, falling under category III as a Monument of Nature (Markoski et al., 2019).

The Duvalo locality is considered to be a volcanic area by local people due to the "rotten eggs" smell, sulfur exhalations, strong soil degassing and "eruptions" from "craters", which are considered a trace of extinct volcanic activity. The presence of "craters", the biggest has a diameter of 50 cm and a depth of 30 cm (Fig. 1d), considered a sign of "volcanic" activity, are instead remnants of the past mining activity. Although the phenomenon was marked as a volcanic solfatara in the local geological literature (e.g. Kotevski, 1987), no volcanic rocks or volcanic activity has been documented in the recent geologic history of the Kosel area (Dumurdzanov & Ivanovski, 1978; Markoski et al., 2019). To support the "volcanic" assumption, during dry periods stronger sulfur smell and whistling sound are present, whilst during wet periods bubbling is the dominant sound (Trojanović, 1925). Furthermore, the area was affected by an increase in its activity with a significant emission of dense smoke, in May 2014. This increase was interpreted as not related to volcanic activity but as the result of filling of the cracks by rainwater, which increased the gas pressure in the subsurface and generated the

This article is protected by copyright. All rights reserved.

Accepted Article

emission of water vapor mixed with other gases (Markoski et al., 2019). The characteristic alterations of the surface are due to the reactions between the exhalations of H_2S and the oxygen dissolved in rainwater, forming sulfuric acid which alters the phyllite rocks, leading to their kaolinitization (Markoski et al., 2019). According to Hoffmann et al. (2010), the phenomenon is related to an active fault system present in the area.

Little research concerning the geochemical characterization of the gas manifestation of the area has been conducted (Trojanović, 1925; Iloski et al., 1957, as cited by Markoski et al., 2019; Dumurdzanov & Ivanovski, 1978). The gases consist of CO_2 (98%), H_2S (0.8%) and inert gases (1%), with a flux rate of 0.2 l s^{-1}. Between 1956 and 1957, in order to ascertain the sulfur reserves of the Duvalo area, the Office for Geological Research – Ohrid drilled two boreholes. An explosion occurred near one of the two boreholes and the analysis of the emitted gases were carried out, showing an increase of H_2S, up to 2% (Iloski et al., 1957, as cited by Markoski et al., 2019).

With the aim to better characterize the source of the Duvalo gas manifestation, the present study reports on new chemical and, for the first time, isotope data of the gas emissions. Furthermore, we present the first map of CO_2 soil diffuse degassing and estimate of the total CO_2 output for the area.

2 Geological setting

The Duvalo site, near Kosel village, is located in the north-eastern part of the Ohrid Basin, that hosts one of the oldest lakes in Europe, Lake Ohrid (Wagner et al., 2008). The Ohrid Basin is a graben structure, part of the Cenozoic South-Balkan Extensional Regime (Burchfiel et al., 2008; Dumurdzanov et al., 2005), that is flanked by active N-S striking normal faults, controlled by E-W extension since Pliocene (Dumurdzanov et al., 2005; Hoffmann et al., 2010), after initial opening as a pull-apart basin in Late Miocene (Lindhorst et al., 2015).

The Ohrid Basin is situated along the contact of two major tectonic units: the Mirdita Ophiolite Zone in the west, and the Western Macedonian Zone (also Korab Zone or West Pelagonian Zone) to the east (Dumurdzanov et al., 2005; Robertson & Shallo, 2000). A recent review by Schmid et al. (2020), places the Mirdita Zone within the Western Vardar ophiolitic units, obducted in Late Jurassic-Early Cretaceous onto the Adriatic margin, with the Korab Zone considered as part of the Upper Pelagonian unit, itself considered as an Adria-derived unit (Fig.1). The Upper Pelagonian is built of Paleozoic metamorphic rocks (various schists classified as a phyllite formation), which are superimposed by Triassic rocks that comprise a clastic-carbonate formation with diabase intrusions and rhyolite lava flows, and a cherty-carbonate formation composed of limestone and dolomite (Dumurdzanov & Ivanovski, 1978).

In the area around Kosel village, rocks of the phyllite formation mostly outcrop, composed of quartz-sericite schist, with lenses of quartz-sericite-graphitic schists, with also small intrusions of granitoids and diabase. To the southeast, Triassic marble tops Galichica Mountain. Duvalo is situated within the quartz-sericite schists, along an intersection of NNW and NNE striking faults (Fig. 2). The latter follows the direction of an active fault within the sediments of Ohrid Lake (Lindhorst et al., 2015). The area is seismically active (Arsovsky & Hadžievsky, 1970; Dumurdzanov et al., 2016), with the most recent significant earthquake, with a magnitude of $M_L = 4.9$, registered nearby in 2017 (Bojadjieva et al., 2019). Strongly influenced by the nearby regions (Albania and Northern Greece), the area of Ohrid is associated with one of

This article is protected by copyright. All rights reserved.

the highest levels of seismic hazard (higher activity rate and maximum magnitude) in the country (Lee and Trifunac, 2017). The highest seismic activity occurs in the southern parts of the Ohrid graben, with notable earthquakes registered in 1906 (Mw = 6.04), 1911 (Mw = 6.68) and 1912 (Mw = 6.04), having epicenters in Ohrid Lake (Dumurdzanov et al. 2016). Hypocenters are shallow with depths between 10 and 25 km, although some earthquakes with depths between 25 and 50 km have been registered in close by areas (Hoffmann et al. 2010). Based on these sparce data, it is inferred that some of the active faults may reach the brittle-ductile transition zone at ~12-25 km depth (Reicherter et al. 2011).

The gas exhalation area at Duvalo is easily recognized by the large zone devoid of vegetation and covered by light colored alteration products, bordered by a dense forest area. The trees at the limit of the exhaling area show chlorotic or necrotic leaves or needles especially on their lower branches. The area is elongated in NNW-SSE direction on the hillside bordering the Ohrid Plain and comprises also some minor areas separated by forest. At about one km north of Duvalo, along the NNW-striking fault, another area devoid of vegetation can be recognized (Kosel 2). Here only a few alteration areas may be found, with quartz-sericite-graphitic schists also exposed, while most of the area is extensively eroded and shows a very steep relief because of the highly erodible rocks. Similarly, the exposed parts of the quartz-sericite-graphitic schists can be found at about 4 km south of Duvalo, at the north-eastern outskirt of Velgoshti village, on a hill (thousands of m^2) covered by sparse stunted vegetation. Here, sulfur and sulfate efflorescence's and incrustations can be recognized along a 50 m stretch at the southern foot of the hill.

3 Materials and Methods

In August 2019 and March 2020, two sampling campaigns were carried out. Nine gas samples were collected in the study area: seven samples have been collected in the Duvalo area and one sample in each of the other two sites with evident alteration signs, Kosel 2 and Velgoshti (Fig. 2). Samples were collected through a probe inserted in the soil at 50 cm depth and stored in glass vessels with two vacuum stopcocks and Exetainer© Labco vials (12 ml of volume). The chemical and isotope analyses were carried out at the laboratories of Istituto Nazionale di Geofisica e Vulcanologia of Palermo (INGV-Palermo).

The concentrations of He, H_2, H_2S, O_2, N_2, CO_2 and CH_4 in the samples were determined using an Agilent 7890B gas chromatograph with Ar as carrier, equipped with a 4-m Carbosieve S II and PoraPlot–U columns. A TCD detector was used to measure the concentrations of He, O_2, N_2 and CO_2 and a FID detector for CH_4. The analytical errors were estimated as less than 5 % for He, H_2, H_2S and C_2H_6 and 3 % for O_2, N_2, CH_4 and CO_2. Argon was analyzed using a Perkin Elmer XL gas-chromatograph with a MSieve 5A column, with the TCD detector having He as carrier.

An evacuated glass vessel filled with a 4M soda solution, which blocked CO_2 and H_2S as dissolved ions, was used to concentrate the minor gases in order to obtain the CH_4/C_2H_6 ratio of Duvalo sample in March 2020.

The $^{13}C/^{12}C$ ratios of CO_2 (expressed as $\delta^{13}C$-CO_2 ‰ vs. V-PDB) were measured using a Finnigan Delta S mass spectrometer after purification of the gas mixture by standard procedures using cryogenic traps (precision ±0.1 ‰). Carbon and hydrogen isotopes of CH_4 were measured using a Thermo TRACE GC interfaced with a Delta Plus XP gas source mass spectrometer,

This article is protected by copyright. All rights reserved.

equipped with a Thermo GC/C III (for carbon) and with GC/TC peripherals (for hydrogen). The $^{13}C/^{12}C$ ratios are reported as $\delta^{13}C\text{-}CH_4$ values (precision ±0.2 ‰) with respect to the V-PDB standard while $^{2}H/^{1}H$ ratios are reported here as $\delta^{2}H\text{-}CH_4$ values (precision ±2.0 ‰) with respect to the V-SMOW standard. The abundance and isotope composition of He, and $^{4}He/^{20}Ne$ ratios, were determined by separately admitting He and Ne into a split flight tube mass spectrometer (Helix SFT). Helium isotope compositions are given as R/R_A, where R is the ($^{3}He/^{4}He$) ratio of the sample and R_A is the atmospheric ($^{3}He/^{4}He$) ratio ($R_A=1.386\times10^{-6}$). The analytical errors were generally <1 %.

The carbon dioxide flux was measured using the accumulation chamber method (Chiodini et al., 1998) at 321 sites with a portable soil fluxmeter (WEST Systems, Italy). Flux values were determined at each site from the rate of CO_2 concentration increase in the chamber and are expressed as grams per square meter per day (g m^{-2} d^{-1}) after conversion from volumetric to mass concentrations considering the measured atmospheric pressure and temperature values. The portable soil fluxmeter is equipped with a Licor LI820 IR spectrometer characterized by a reproducibility better than 20 % in the measuring range 10 - 20,000 ppm. The used accumulation chamber has an area of 0.031 m^2 and a volume of 0.0028 m^3. Care was taken to follow the recommendations regarding instrument calibration, flux measurements and data elaboration as proposed by Lewicki et al. (2005). The entire dataset is reported in Table A1 (Appendix).

The CO_2 flux data were derived using statistical and geostatistical tools. To characterize the CO_2 flux the GSA method (Chiodini et al., 1998), based on Sinclair's partitioning method (Sinclair, 1974), was used. This method allows the partitioning of a polymodal statistical distribution into individual populations and the definition of the populations' statistical parameters and relative proportions. Because the gas flux data resulted a combination of log-normal distributed populations, the computed mean and standard deviation of the partitioned populations refer to the logarithm of CO_2 flux values. The mean of the CO_2 flux and the 95% confidence interval of the mean were thus estimated by the Sichel's t-estimator (David, 1977).

A map of the CO_2 fluxes was drawn using the sequential Gaussian simulations (sGs method; Cardellini et al., 2003). The sGs method consists of the production of numerous equiprobable realizations of the spatial distribution of the CO_2 flux using the sgsim algorithm of the GSLIB software library (Deutsch & Journel, 1998) according to the variogram model of the normal score of the CO_2 flux derived from the experimental variogram. One hundred equiprobable realizations were computed for the area using a computational grid of 2×2 m. The CO_2 flux map is then reported as map of the ''expected'' values at any cell (E-type estimates), obtained through a pointwise linear average of all the realizations (Deutsch & Journel, 1998). The results of the sGs were also used to estimate the total CO_2 output, summing the products of simulated value at each grid cell by the cell surface. The mean and the standard deviation of the 100 simulated values of total CO_2 output, computed for the 100 realizations, were assumed to be the characteristic values of the CO_2 output of its uncertainty for the area.

The soil temperature was measured at 50 cm depth by means of a digital thermocouple (error ±0.3 °C in the range from -100 to 200 °C) only at five sites in August 2019.

4 Results

The chemical and isotope composition and geographic coordinates of the gas samples are reported in Table 1. Generally, carbon dioxide, in four samples, and nitrogen and oxygen, in

This article is protected by copyright. All rights reserved.

three samples, are the dominant components of the gas samples from the Duvalo area (Fig 3). Carbon dioxide arrives up to 966,100 μmol mol^{-1}, N_2 ranges from 17,900 to 736,100 μmol mol^{-1}, and O_2 concentrations vary between 128 and 189,700 μmol mol^{-1}, indicating sometimes an important air component. The gases collected at Kosel 2 and Velgoshti are dominated by the atmospheric component (N_2 and O_2), while CO_2 concentrations range from 2,900 to 8,700 μmol mol^{-1}, respectively. For all samples, hydrogen sulfide concentrations show a wide spectrum of values between <10 and 5500 μmol mol^{-1}. Methane concentrations display also a large range, that varies between 11 and 3250 μmol mol^{-1}. Minor compounds, hydrogen and helium, are also found, with concentrations of <3 - 1010 μmol mol^{-1} for the former and <3 - 70 μmol mol^{-1} for the latter. Ethane is always below the detection limit (< 10 μmol mol^{-1}) but the CH_4/C_2H_6 ratio (513) was measured in one sample in the enriched headspace gas of a soda ampule. Argon was measured only in few samples and showed absolute values and N_2/Ar ratios close to the atmospheric values in the samples of Kosel 2 and Velgoshti. On the contrary, Duvalo samples showed very low concentrations of argon (61 and 79 μmol mol^{-1}) and N_2/Ar ratios (> 200) higher than atmospheric values.

The $\delta^{13}C_{CO2}$ at Duvalo ranges from -0.2 to 2.7 ‰ vs. V-PDB, whilst Kosel 2 and Velgoshti have values of -13.7 and -0.8 ‰, respectively. The isotope composition of He was determined only in two samples from Duvalo, both having the value of 0.10 R/R_A. The isotope composition of CH_4 has also been determined showing $\delta^{13}C_{CH4}$ values that range from -36.8 to -34.4 ‰ V-PDB and $\delta^{2}H_{CH4}$ values that vary between -180 and -158 ‰ vs. V-SMOW.

Soil CO_2 fluxes measured in the Duvalo area range from 1.34 to 59,300 g m^{-2} d^{-1} and were modeled as the combination of three log-normal populations (Fig. 4), for which statistical parameters are reported in Table 2.

This article is protected by copyright. All rights reserved.

The populations B and C are characterized by elevated mean CO_2 flux values and may be considered to represent deep CO_2 degassing. The occurrence of two populations for the deep CO_2 degassing could reflect the relative prevalence of diffusive or advective CO_2 transport mechanisms (e.g., Chiodini et al., 2020). On the contrary, population A is characterized by a relatively low mean CO_2 flux and may represent the biological CO_2 background flux for the area. The mean CO_2 flux of population A (45 g m^{-2} d^{-1}) is actually slightly higher than the CO_2 fluxes produced by the biological activity for different ecosystems presented in other studies (mean CO_2 flux from 0.2 g m^{-2} d^{-1} to 21 g m^{-2} d^{-1}, Cardellini et al. 2017, Viveiros et al., 2010 and reference therein) and relatively high with respect to the biological background generally found in numerous hydrothermal sites (Chiodini et al., 2008 and references therein). However, a relatively high biological background CO_2 flux has also been reported for several sites; for example, mean background CO_2 fluxes of 44.8 g m^{-2} d^{-1} and 46.85 g m^{-2} d^{-1}were reported at the Furnas do Enxofre degassing area (Azores; Viveiros et al., 2020) and at Horseshoe Lake (Mammoth Mountain, CA, Cardellini et al., 2003) respectively.

Temperatures were in the range of 17.2 – 18.5 °C, higher than the mean annual atmospheric temperature of the area (11.1 °C; Zikov 1997), but close to the mean summer atmospheric temperature (19.7 °C; Zikov 1997) and lower than the atmospheric temperatures during the measurement campaign (from about 20 °C in the early morning up to about 40 °C in the afternoon).

Only two soil CO_2 flux measurements were made at Kosel 2 in areas with some signs of soil alteration, and in both cases low CO_2 flux values were measured (4.61 and 5.23 g m^{-2} d^{-1}). No flux measurement was made at the Velgoshti site.

5 Discussion

5.1 Origin of the gases

The most CO_2-rich samples are consistent with previous analyses in 1925 (Trojanović, 1925), 1957 (Iloski et al., 1957; as reported in Markoski et al. 2019) and in 1977 (in Markoski et al., 2019), when it was reported that the gases were composed mainly of CO_2 (90-98%) and H_2S (0.8%). The consistency of the results indicates a certain stability of the exhaling system, at least in the last century.

Here, isotope analyses were carried out to deduce the origin of the gas manifestations in the Duvalo area. Helium compositions have a R/R_A ratio of 0.1, which indicates an almost pure crustal origin (Fig. 5a). Deep normal or transcurrent faults may act as a preferential pathway for upwelling of mantle helium, which may be recognized in R/R_A values tending towards MORB values (8±1 R/R_A - Ozima & Podosek, 2002). The Ohrid area is a seismically active extensional basin and the site of Duvalo corresponds to an active fault system. Such extensional basins are widespread in the neighboring areas. For the other tectonically similar areas in the south and in the north-west of the country, mantle contributions up to 20% (R/R_A up to 1.64) have been measured (Fig. 5a - Temovski et al., 2020). Similarly high R/R_A values (up to 1.27) have been found also in northern Greece (Fig. 5a - Daskalopoulou et al., 2018). On the contrary, at Duvalo a mantle contribution seems absent or at least trivial (about 1%). Similarly, $\delta^{13}C$-CO_2 values between -0.8 and -0.1 ‰ and $CO_2/^3He$ ratios between 7.6×10^{10} and 8.4×10^{10} point towards an

This article is protected by copyright. All rights reserved.

almost pure crustal (marine limestones) source also for CO_2, with at most 2% mantle contribution (Fig. 5b).

Data have been plotted in $\delta^{13}C$-CH_4 vs. $\delta^{2}D$-CH_4 (Schoell, 1983) and $CH_4/(C_2+C_3)$ vs. $\delta^{13}C$-CH_4 (Bernard et al., 1977) space, modified by Milkov and Etiope (2018) in order to discriminate the origin of methane (Fig. 6). The Duvalo samples fall within the thermogenic range, although secondary microbial or oxidation processes cannot be excluded (Milkov & Etiope, 2018 and reference therein).

The origin of H_2S in the gases released at Duvalo is somewhat harder to constrain. Unfortunately, no sulfur isotope data are available at present. H_2S is a typical gas of hydrothermal origin but in the present case we have no indication about the presence of a hydrothermal system at depth. No thermal springs are present at Duvalo or in the surrounding area. The closest thermal springs are more than 40 km away to NW. No thermal anomaly has been recognized within the soils of Duvalo and at 50 cm depth, even at the sites with the highest measured CO_2 fluxes, the soil temperatures were close to the mean annual atmospheric temperature of the area. The absence of thermal anomalies and the low temperature of the gases is not in itself an indication of absence of any geothermal system at depth. Nevertheless, the south-western part of Macedonia, to which the area belongs, is not considered to have anomalous heat flow (Popovska-Vasilevska & Armenski, 2016).

An alternative process that might produce H_2S is sulfate reduction (Machel, 2001), either microbially (MSR) or thermochemically (TSR). In both cases, the process can be schematized by the following reaction:

$$\text{Hydrocarbons} + CaSO_4 \rightarrow CaCO_3 + H_2S + H_2O \pm CO_2 \pm \text{altered hydrocarbons} \pm \text{solid bitumen.}$$

MSR is considered to occur at temperatures below 80°C while TSR generally in the 100-140°C range (Machel, 2001). TSR is thermodynamically favored, but kinetically limited, also at temperatures down to 25 °C (Mougin et al., 2007).

In the study area, no hydrocarbon, gypsum or anhydrite deposits have been identified, either outcropping or in the subsoil. Nevertheless, organic-rich schists are present in the metamorphic basement part of the Upper Pelagonian in the area (Dumurdzanov & Ivanovski, 1978). Shists may be the origin of some hydrocarbons, and the CH_4 found in the gases released at Duvalo. The isotopic composition of the CH_4 suggests a thermogenic origin compatible with TSR processes (Milkov and Etiope, 2018). Despite their absence at the surface in the area of Duvalo, gypsum or anhydrite deposits may be present at depth. As suggested by Frasheri et al. (1996), the Peshkopi tectonic window in Albania to the north, which is part of the Ionian zone and underlies the Upper Pelagonian (Fig.1; Robertson & Shallo, 2000; Schmid et al., 2020), comprises Triassic evaporites in its sequence. Evaporite sulfates are also found south of Peshkopi, on the Macedonian side, near Debar (Fig. 1; Jančev et al., 1999). Furthermore, sulfates may be contained in small quantities in shallow water carbonates (generally dolomites) of the sedimentary sequence of the Upper Pelagonian. Although not identified, one of these sulfate-containing sequences may be present at some depth beneath Duvalo.

This article is protected by copyright. All rights reserved.

Accepted Article

Due to the active tectonic structures of the area, the sulfate-bearing strata may have been put in contact with the organic-rich shales by the fault system along the eastern part of the Ohrid graben. Even without anomalous heat fluxes, the most favorable temperature conditions for TSR may be reached at depths between 3 and 4 km considering an average geothermal gradient (30 °C km^{-1}). The H_2S produced rises towards the surface through the same fault system either in the gas phase or dissolved in water. During transport, H_2S could be oxidized by oxygen-charged meteoric waters, producing H_2SO_4. The strongly acidic solutions that will form may react with the limestones of the sedimentary sequence, producing abundant CO_2.

Sulfuric acid may also be produced by the oxidative weathering of sulfides. In the geologic succession of the study area, sulfides (mainly pyrite) are found within the phyllite formation, at the contact with the granitoid intrusions (Dumurdzanov & Ivanovski, 1978) and may contribute to the production of the CO_2 released at Duvalo. Nevertheless, oxidation of sulfide minerals cannot explain the presence of H_2S in the released gases. Metamorphic reactions producing H_2S from sulfide minerals require high temperatures (> 450 °C) and/or high pressures (Tomkins, 2010) and are therefore an improbable H_2S source for this system.

5.2 Processes affecting gas composition in the soil

Sample compositions are plotted on a N_2-O_2-CO_2 ternary diagram (Fig. 3), which shows a mixing trend between a CO_2-dominated component (with CO_2 concentrations > 960,000 μmol mol^{-1}) and an atmospheric air component. Such a trend is typical of soil gases where low CO_2 contents correspond to low flux rates of the deep-derived gases (Fig. 3). The N_2 excess with respect to the atmospheric air ratio in the soil gas sample of Velgoshti may be attributed to oxygen consumption given that the N_2/Ar ratio of the same sample is nearly identical to the atmosphere. Helium, CH_4 and H_2S are almost completely related to the deep geogenic member; the highest values being found in the sample with the highest CO_2 concentration (Fig. 7). In a binary plot vs. CO_2, both CH_4 and He are mostly aligned along a mixing line with atmospheric air. Small deviations from the mixing line may derive from solubility differences when the uprising gases pass through groundwater not saturated in these gases. Few samples have CH_4 well below the mixing line indicating loss by microbial or inorganic oxidation. For H_2S, only the samples with a very low air contribution approximately follow the mixing line. Samples with ≥50% of air contribution display H_2S values at or below the detection limit (10 μmol mol^{-1}), orders of magnitude beneath the mixing line. On its transit towards the soil surface, H_2S can be lost either by dissolution in water (higher solubility with respect to CO_2) or, more importantly, by oxidation. A higher contamination of the soil gases by air is, generally, connected with lower fluxes and therefore to higher permanence time in the soil, favoring oxidation processes. The result of H_2S oxidation is the deposition and accumulation of sulfate alteration minerals in the soil (Alpers et al., 2000).

Kosel 2 displays a soil gas composition close to that of atmospheric air, indicating the absence of significant deep gas exhalations. The limited alteration of the soil there may be related to the physical-chemical weathering of pyrite in the outcropping black shales (Dumurdzanov & Ivanovski, 1978). Pyrite oxidation is consistent with the low pH (~3) of the water in the small creek draining this area. Like Duvalo, the area of Kosel 2 is also crossed by some active tectonic structures (Fig. 2) and we cannot exclude that is has been the site of geogenic degassing in the past. Nevertheless, the areas devoid of vegetation in this area are all

This article is protected by copyright. All rights reserved.

very steep and are probably characterized by strong physical weathering and are not the consequence, like in Duvalo, of intense chemical alteration.

The Velgoshti sample has a higher N_2/O_2 ratio (6.1) with respect to air, which can be attributed to oxygen consumption. Although the altered soil covers a much larger area than in Kosel 2, we have no flux measurement that indicates that such alteration is linked to high gas fluxes, as in Duvalo. Our single soil gas analysis does not indicate a geogenic contribution. Nevertheless, the area deserves future study of soil CO_2 fluxes.

5.3 CO_2 flux mapping and CO_2 output estimation

An estimation of CO_2 release from soil degassing has been obtained following the sGs method (Cardellini et al., 2003). The experimental variogram of the normal scores of CO_2 flux (Fig. 8b) highlights two nested structures: one characterized by a shorter range (30 m) and one by a larger range (90 m), that may reflect the occurrence of a set of spatially organized small scale anomalies. The map of the CO_2 flux shows (Fig 8a) that the most anomalous degassing areas are aligned along preferential directions following the main tectonic lineament of the area. We infer that fracture-zones channel the deep gas, described also as Diffuse Degassing Structures (DDS, Chiodini et al., 2001). Significant soil CO_2 degassing can help to detect active tectonic features as shown by Lewicki & Brantley (2000), Kämpf et al. (2013), Weinlich (2014), and Kis et al. (2017), among others. The inferred features are in concordance with the lineaments showed by Dumurdzanov & Ivanovski (1978) mainly in the NNW-SSE direction but also in the NNE-SSW or NE-SW directions.

The total amount of released CO_2 estimated from the sGs results for the Duvalo site is 66.9 t d^{-1} ± 7.1 t d^{-1} from the mapped area of ~54,550 m^2. This CO_2 output corresponds mainly to deep CO_2, with a maximum contribution of biogenic CO_2 of 2.4 t d^{-1} assuming a biogenic CO_2 flux of 45 g m^{-2} d^{-1} (i.e. the mean CO_2 flux of population A) constant over all the area.

5.4 Duvalo in the regional context

The Balkan and the nearby Italian peninsulas, due to their intense geodynamic activity, are sites of widespread geogenic degassing. But while Italy has been widely studied in the last decades (e.g., Frondini et al., 2019 and reference therein; Rogie et al., 2000; Chiodini et al., 2011), much less information is available for the Balkans. The latter is long known to be the site of countless CO_2-rich gas manifestations but relatively few have been studied to unravel the origin of the gases (Italiano et al., 2017; Marinkovic et al., 2012; Piperov et al., 1994; Randazzo et al., 2021; Vaselli et al., 2002). The best studied region up to now is probably Greece, the southern end of the Balkan Peninsula (Daskalopoulou et al., 2018, 2019). Even fewer studies have attempted to quantify the CO_2 output of these sites (Kis et al., 2017; Nisi et al., 2013) with the exception of those in Greece, which were recently reviewed by Daskalopoulou et al. (2019). The studied degassing systems in Greece are almost all connected to recent (Quaternary) or active volcanic activity. The output obtained here for the non-volcanic Duvalo site is comparable to the estimated CO_2 outputs of the active volcanic systems of the Aegean arc, which range from 2.6 t d^{-1} at Methana (D'Alessandro et al., 2008) to 92 t d^{-1} at Nisyros (Bini et al., 2019). Non-volcanic degassing has been detected also in Greece but until now only that of the Sperchios Basin area has been estimated, at about 27 t d^{-1} (D'Alessandro et al., 2020). The area of Florina has probably an even higher total CO_2 output, but it has not yet been quantified. Evidence of high CO2 fluxes here comes from the extraction, by the Air Liquide Greece Company of about

This article is protected by copyright. All rights reserved.

Accepted Article

80 t CO_2 per day from deep wells without apparently affecting the output of the numerous gas manifestations of the area (Pearce et al., 2004). Furthermore, the anomalous degassing area of Florina extends beyond the border with North Macedonia into the Bitola Plain where other companies exploit the CO_2 accumulation in the subsoil (Mirčovski et al., 2015).

In Italy many non-volcanic gas manifestations are present and most have been studied, both to define the origin of the emitted gases and to quantify their CO_2 output (e.g. Chiodini et al., 1999, 2011, 2020; Frondini et al., 2008, 2012; Minissale et al., 1997; Rogie et al., 2000). Many of them have higher CO_2 outputs (e.g. Chiodini et al., 2011, 2020) with respect to Duvalo, sometimes up to more than one order of magnitude (e.g. Mefite D'Ansanto 2000 t d^{-1}; Chiodini et al., 2010). But in both cases, for the Italian sites and for the Greek ones, a direct or indirect connection to the mantle is always hypothesized. In the case of Central Italy helium isotope compositions range from values around 2 R/R_A to about 0.02 R/R_A. The highest $^3He/^4He$ ratios resemble the values measured in the olivine and pyroxenes of the Tuscan–Latium volcanic products (Martelli et al., 2004), linked to subduction-related carbon-rich mantle (e.g. Frezzotti et al., 2009; Martelli et al., 2004; Peccerillo, 1999), and the lower ones are interpreted as evidence for variable addition of crustal ^4He during the gas storage in crustal reservoir (e.g., Chiodini et al., 2011). Also in the case of Greece, $^3He/^4He$ up to 1.3 R/R_A point to substantial gas contributions from the mantle (Daskalopoulou et al., 2019).

In the case of Duvalo the contribution from the mantle seems absent or at least very low, if a MORB-type mantle end-member is assumed. A subcontinental lithospheric mantle (SCLM) type (Gautheron & Moreira, 2002) source has been hypothesized for gas manifestations in two areas at the periphery of the Balkan peninsula: Slovenia (Bräuer et al., 2016) and the South Aegean Active Volcanic Arc (Shimizu et al., 2005). Nevertheless, these hypotheses have not been confirmed by data on fluid inclusions in mantle minerals and in the second case they have been challenged by recent data from Kolumbo volcano whose gas emissions have He and C isotopic compositions compatible with a MORB-type mantle (Rizzo et al., 2016).

Furthermore, widespread mantle metasomatism by fluids released by the subducting slab in the central Mediterranean region has been hypothesized from isotopic composition of gas manifestations (Chiodini et al., 2011; Frondini et al., 2019; Parello et al., 2000), mantle xenoliths' fluid inclusions (Martelli et al., 2004) and petrological and geophysical data (Frezzotti et al., 2009). One of the best studied systems is the island of Stromboli where fluid inclusions in minerals of mantle xenoliths define the mantle end-member for both He (Martelli et al., 2014) and C (Gennaro et al., 2017) isotopes (Fig. 5). Even stronger metasomatism has been hypothesized in the Roman Magmatic Province (central Italy) from the He isotopic composition (0.44–1.73 R/R_A, Martelli et al. 2004) measured in fluid inclusions trapped within olivine and pyroxene phenocrysts associated with mantle-derived basic lavas and pyroclastic rocks.

Some evidence of a metasomatized mantle beneath the southern Balkan Peninsula may come from the R/R_A values measured in gas manifestations never exceeding 1.6 in North Macedonia (Temovski et al., 2020), 1.3 in continental Greece (Daskalopoulou et al., 2018) and 0.8 in Bulgaria (Piperov et al., 1994). Furthermore, mantle metasomatism by subducting material was also invoked by Yanev et al. (2008) in their petrographic study of the Miocene to Pleistocene volcanic rocks of North Macedonia. Finally, Molnar et al. (2021), analyzing fluid inclusions in olivine phenocrysts from the Mlado Nagoričane volcanic center (North Macedonia), measured R/R_A values in the range of 3.1-4.5. These results are well below MORB

This article is protected by copyright. All rights reserved.

or SCLM values and may also suggest a metasomatic process within the mantle below North Macedonia.

As seen from central Italy, a strongly metasomatized mantle would have He and C-isotopic values very different from a MORB-type mantle, leading to a severe underestimation of the mantle contribution in the sampled gases. However, even considering a metasomatized mantle like central Italy, the mantle contribution at Duvalo would be still low (< 10%). Nevertheless, should the low or absent contribution from mantle degassing be confirmed by future studies, this would make Duvalo a very peculiar system: a relatively shallow source within the crust able to sustain fluxes of CO_2 higher than 1000 t km^{-2} d^{-1}.

6 Conclusions

The area of Ohrid is a seismically active extensional basin and the site of Duvalo corresponds to an active fault system. The Duvalo area exhibits a natural phenomenon of intense soil degassing considered as a volcanic solfatara in the local geological literature, although volcanic rocks or volcanic activity have not been found in the area. Based on the isotopic composition of the gas manifestations, we propose a tectonic origin for the phenomena. The isotope composition of helium and $\delta^{13}C$-CO_2 indicate an almost pure crustal (marine limestone) origin and mantle contribution seems absent or at most trivial (about 1%).

The presence of H_2S may be explained by thermochemical sulfate reduction (TSR), which is compatible with the isotopic composition of methane that falls within the thermogenic range. Due to the strong displacement of the tectonic structures of the area, the sulfate-bearing strata may have been put in contact with the organic-rich shales of metamorphic basement by the fault system along the eastern part of the Ohrid graben. Part of the uprising H_2S may be oxidized by oxygen-charged meteoric waters in the shallower part of the system and the sulfuric acid thus produced may react with carbonate rocks, producing abundant CO_2 with the isotopic composition measured at Duvalo.

A map of CO_2 flux is shows that the most anomalous degassing areas are aligned along a NNW-SSE direction following the main tectonic lineament direction of the area. The total amount of released CO_2 for the non-volcanic Duvalo site is estimated at 66.9 t d^{-1}. The CO_2 output obtained is comparable to, albeit slightly less than the volcanic and non-volcanic systems of Greece and Italy. Nevertheless, the peculiarity of the Duvalo system lies in its ability to sustain high CO_2 fluxes (> 1000 t km^{-2} d^{-1}) with a relatively shallow crustal source.

Acknowledgments

This research was funded by DCO Grant n. 10881-TDB “Improving the estimation of tectonic carbon flux”, by the European Social Fund (PO FSE Sicilia 2014-2020) in the frame of the project “Metodi di controllo geochimico e geofisico dei fenomeni naturali sul campo ed in laboratorio” (CUP: G77B17000200009), by the Italian Ministero Istruzione Università e Ricerca (MIUR, under Grant PRIN2017-2017LMNLAW “Connect4Carbon”), and was supported by the European Union and the State of Hungary, co-financed by the European Regional Development Fund in the project of GINOP-2.3.2-15-2016-00009 “ICER”. Fieldwork was carried out under Research Permits Nos. UP1-11/1-691/2019 and UP1-11/1-1829/2019 issued by the Ministry of Environment and Physical Planning of the Republic of North Macedonia.

This article is protected by copyright. All rights reserved.

Accepted Article

The authors thank INGV-Palermo for supporting the analyses carried out in its laboratories and the technicians and responsibles (Giorgio Capasso, Fausto Grassa, Ygor Oliveri, Andrea Rizzo, Aldo Sollami, Francesco Salerno and Mariano Tantillo) for their analytical contribution. We are also indebted with Felipe Aguilera, Agnes Mazot, an anonymous reviewer and the editor Marie Edmonds for their critical comments which contributed to improve the manuscript.

Open Research

Li Vigni, L., Cardellini, C., Temovski, M., Ionescu, A., Molnar, K., Palcsu, L., Gagliano, A. L., Cappuzzo, S., D'Alessandro, W., 2022. Location, chemical and isotopic composition of soil gases collected in Duvalo area, North Macedonia., Version 1.0. Interdisciplinary Earth Data Alliance (IEDA). https://doi.org/10.26022/IEDA/112209. Accessed 2022-01-11
Li Vigni, L., Cardellini, C., Temovski, M., Ionescu, A., Molnar, K., Palcsu, L., Gagliano, A. L., Cappuzzo, S., D'Alessandro, W., 2022. Location and soil CO2 flux from Duvalo area, North Macedonia., Version 1.0. Interdisciplinary Earth Data Alliance (IEDA). https://doi.org/10.26022/IEDA/112210. Accessed 2022-01-11.

References

Alpers, C.N., Jambor, J.L., & Nordstrom, D.K. eds. (2000). Sulfate Minerals – Crystallography, Geochemistry and Environment Significance. *Reviews in Mineralogy and Geochemistry*, *40*, 608pp.

Arsovsky, M., & Hadžievsky, D. (1970). Correlation between neotectonics and the seismicity of Macedonia. *Tectonophysics, 9*, 129-142.

Barnes, I., Irwin, W.P., & White, E. (1978). Global Distribution of Carbon-Dioxide Discharges and Major Zones of Seismicity, Scale 1:40,000,000. *U.S. Geological Survey Water Resourches Investigation Report*. WRI 78-39.

Bernard, B., Brooks, J.M., & Sackett, W.M. (1977). A geochemical model for characterization of hydrocarbon gas sources in marine sediments. *Offshore Technology Conference*, OTC-2934-MS

Berner, R.A., & Lasaga, A.C. (1989). Modeling the geochemical carbon cycle. *Scientific American, 260*, 74-81.

Bini, G., Chiodini, G., Cardellini, C., Vougioukalakis, G.E., & Bachmann, O. (2019). Diffuse emission of CO_2 and convective heat release at Nisyros caldera (Greece). *Journal of Volcanology and Geothermermal Research, 376*, 44–53.

Bojadjieva, J., Sheshov, V., Edip, K., Chaneva, J., Kitanovski, T., & Ivanovski, D. (2019). GIS-based assessment of liquefaction potential for selected earthquake scenarios. In: Silvestri F.,

This article is protected by copyright. All rights reserved.

Accepted Article

Moraci N. (eds). *Earthquake Geotechnical Engineering for Protection and Development of Environment and Constructions. Proceedings in Earth and Geosciences, vol. 4*, 1453-1460.

Brantley, S.L., & Koepenick, K.W. (1995). Measured carbon dioxide emissions from Oldoinyo Lengai and the skewed distribution of passive volcanic fluxes. *Geology, 23*, 933–936.

Bräuer, K., Geissler, W.H., Kämpf, H., Niedermannn, S., & Rman, N. (2016). Helium and carbon isotope signatures of gas exhalations in the westernmost part of the Pannonian Basin (SE Austria/NE Slovenia): Evidence for active lithospheric mantle degassing. *Chemical Geology, 422*, 60–70.

Brune, S., Williams, S., & Müller, D. (2017). Potential links between continental rifting, CO_2 degassing and climate change through time. *Nature Geoscience, 10*, 941–947.

Burchfiel, B.C., Nakov, R., Dumurdžanov, N., Papanikolaou, D., Tzankov, T., Serafimovski, T., King, R.W., Kotzev, V., Todosov, A., & Nurce, B. (2008). Evolution and dynamics of the Cenozoic tectonics of the South Balkan extensional system. *Geosphere, 4*, 919–938.

Burton, M.R., Sawyer, G.M., & Granieri, D. (2013). Deep carbon emissions from volcanoes. In: Carbon in Earth (Hazen R.M., Jones A.P., Baross J.A., eds.) *Reviews in Mineralogy and Geochemistry, 75*, 323–355.

Cardellini, C., Chiodini, G., & Frondini, F. (2003). Application of stochastic simulation to CO_2 flux frim soil: mapping and quantification of gas release. *Journal of Geophysical Research*, 108, 2425.

Cardellini, C., Chiodini, G., Frondini, F., Avino, R., Bagnato, E., Caliro S., Lelli, M., & Rosiello, A. (2017). Monitoring diffuse volcanic degassing during volcanic unrest: the case of Campi Flegrei (Italy). *Scientific Report*, 7, 6757.

Chiodini, G., Cioni, R., Guidi, M., Raco, B., & Marini, L. (1998). Soil CO_2 flux measurements in volcanic and geothermal areas. *Applied Geochemistry, 13*, 543–552.

Chiodini, G., Fondini, F., Kerrick, D.M., Rogie, J., Parello, F., Peruzzi, L., & Zanzari, A.R. (1999). Quantification of deep CO_2 fluxes from central Italy: examples of carbon balance for regional aquifers and soil degassing. *Chemical Geology, 159*, 205–222.

Chiodini, G., Frontini, F., Cardellini, C., Parello, F., & Peruzzi, L. (2000). Rate of diffuse carbon dioxide Earth degassing estimated from carbon balance of regional aquifers: the case of central Apennine, Italy. *Journal of Geophysical Research, 105*(B4), 8423–8434.

This article is protected by copyright. All rights reserved.

Chiodini, G., Granieri, R., Avino, S., Caliro, S., Costa, A., & Werner, C. (2005). Carbon dioxide diffuse degassing and estimation of heat release from volcanic and hydrothermal systems. *Journal of Geophysical Research, 110*, B08204.

Chiodini, G., Granieri, D., Avino, R., Caliro, S., Costa, A., Minopoli, C., & Vilardo, G. (2010). Nonvolcanic CO_2 Earth degassing: case of Mefite d'Ansanto (southern Apennines), Italy. *Geophysical Research Letters, 37*, L11303.

Chiodini, G., Caliro, S., Cardellini, C., Frondini, F., Inguaggiato, S., & Matteucci, F. (2011). Geochemical evidence for and characterization of CO_2 rich gas sources in the epicentral area of the Abruzzo 2009 earthquakes. *Earth and Planetary Science Letters, 304*, 389–398.

Chiodini, G., Cardellini, C., Di Luccio, F., Selva, J., Frondini, F., Caliro, S., Rosiello, A., Beddini, G., & Ventura, G. (2020). Correlation between tectonic CO_2 Earth degassing and seismicity is revealed by a 10-year record in the Apennines, Italy. *Science Advances, 6*, eabc2938.

D'Alessandro, W., Brusca, L., Kyriakopoulos, K., Michas, G., & Papadakis, G. (2008). Methana, the westernmost active volcanic system of the south Aegean arc (Greece): insight from fluids geochemistry. *Journal of Volcanology and Geothermermal Research, 178*, 818–828.

D'Alessandro, W., Li Vigni, L., Gagliano, A.L., Calabrese, S., Kyriakopoulos, K., & Daskalopoulou, K. (2020). CO_2 release to the atmosphere from thermal springs of Sperchios Basin and northern Euboea (Greece): The contribution of "hidden" degassing. *Applied Geochemistry, 119*, 104660, doi:10.1016/j.apgeochem.2020.104660

Daskalopoulou, K., Calabrese, S., Grassa, F., Kyriakopoulos, K., Parello, F., Tassi, F., & D'Alessandro, W. (2018). Origin of methane and light hydrocarbons in natural fluid emissions: a key study from Greece. *Chemical Geology, 479*, 286-301.

Daskalopoulou, K., Calabrese, S., Gagliano, A.L., & D'Alessandro, W. (2019). Estimation of the geogenic carbon degassing of Greece. (Greece): The contribution of "hidden" degassing. *Applied Geochemistry, 106*, 60-74.

David, M. (1977). *Geostatistical ore reserve estimation*. Developments in Geomathematics 2. Elsevier, Amsterdam, 364 pp

Delmelle, P., & Stix, J. (1999). Volcanic gases. In: *Encyclopedia of Volcanoes*. Academic Press, Sigurdsson H., Houghton B.F., McNutt S.R., Rymer H., Stix J. Eds

This article is protected by copyright. All rights reserved.

Accepted Article

Deutsch, C.V., & Journel, A.G. (1998). GSLIB: *Geostatistical Software Library and User's Guide*. 2nd edition. Oxford University Press, New York.

Dumurdzanov, N., & Ivanovski, T. (1978). Map and explanatory notes of the basic geological map 1:100000 (map sheets Ohrid and Pogradec) of the Socialist Federal Republic of Yugoslavia, Federal Geological Survey, Belgrad, 51.

Dumurdzanov, N., Serafimovski, T., & Burchfiel B.C. (2005). Cenozoic tectonics of Macedonia and its relation to the South Balkan extensional regime. *Geosphere, 1*, 1–22.

Dumurdzanov N., Milutinovic Z, Salis R. (2016): Seismotectonic zones and seismic hazard in the Republic of Macedonia. In: Lepitkova S., Boev, B. (Eds.), *Proceedings of the Third Congress of Geologists of Republic of Macedonia, Geologica Macedonica, Special edition* 4, Vol. 1, 477-491.

Faulkner, D.R., Jackson, C.A.L., Lunn, R.J., Schlische, R.W., Shipton, Z.K., Wibberley, C.A.J., & Withjack, M.O. (2010). A review of recent developments concerning the structure, mechanics and fluid flow properties of fault zones. *Journal of Structural Geology, 32*, 1557–1575.

Fischer, T.P., Arellano, S., Carn, S., Aiuppa, A., Galle, B., Allard, P., Lopez T., Shinohara H., Kelly P., Werner C., Cardellini C., & Chiodini G. (2019). The emissions of CO_2 and other volatiles from the world's subaerial volcanoes. *Science Reports, 9*(1), 18716. https://doi.org/10.1038/s41598-41019-54682-41591

Fischer, T.P., & Aiuppa, A. (2020). AGU Centennial Grand Challenge: Volcanoes and deep carbon global CO_2 emissions from subaerial volcanism—Recent progress and future challenges. *Geochemistry Geophysics Geosystems, 21*, e2019GC008690. https://doi.org/10.1029/2019GC008690

Frasheri, A., Nishani, P., Bushati, S., & Hyseni, A. (1996). Relationship between tectonic zone of the Albanides, based on results of geophysical studies. In: Ziegler, P.A., Horwath, F. (Eds.), *Peri-Tethys Memoir 2: Structure and Prospects of Alpine Basins and Forelands*. *Memoir Musee Historie Naturel, Paris, 170*, 485–511.

Frezzotti, M.L., Peccerillo, A., & Panza, G. (2009). Carbonate metasomatism and CO_2 lithosphere–asthenosphere degassing beneath the Western Mediterranean: an integrated model arising from petrological and geophysical data. *Chemical Geology, 262*, 108–120.

This article is protected by copyright. All rights reserved.

Accepted Article

Frondini, F., Caliro, S., Cardellini, C., Chiodini, G., Morgantini, N., & Parello, F. (2008). Carbon dioxide degassing from Tuscany and Northern Latium (Italy). *Global and Planetary Change, 61*, 89–102, https://doi.org/10.1016/j.gloplacha.2007.08.009

Frondini, F., Cardellini, C., Caliro, S., Chiodini, G., & Morgantini, N. (2012). Regional groundwater flow and interactions with deep fluids in western Apennine: the case of Narni–Amelia chain (Central Italy). *Geofluids, 12*, 182–196.

Frondini, F., Cardellini, C., Caliro, S., Beddini, Rosiello, A., & Chiodini, G. (2019). Measuring and interpreting CO_2 fluxes at regional scale: the case of the Apennines, Italy. *Journal of the Geological Society, 176*, 408-416.

Gautheron, C., & Moreira, M. (2002). Helium signature of the subcontinental lithospheric mantle. *Earth and Planetary Science Letters, 199*, 39–47.

Gennaro, M.E., Grassa, F., Martelli, M., Renzulli, A., & Rizzo, A.L. (2017). Carbon isotope composition of CO_2-rich inclusions in cumulate-forming mantle minerals from Stromboli volcano (Italy). *Journal of Volcanology and Geothermermal Research, 346*, 95–103.

Hoffmann, N., Reicherter ,K., Fernández-Steeger, T., & Grützner, C. (2010). Evolution of ancient Lake Ohrid: a tectonic perspective. *Biogeosciences, 7*, 3377-3386.

Hunt, J.A., Zafu, A., Mather, T.A., Pyle, D.M., & Barry, P.H. (2017). Spatially variable CO_2 degassing in the main Ethiopian rift: implications for magma storage, volatile transport, and rift-related emissions. *Geochemistry Geophysics Geosystems, 18*, 3714–3737.

IPCC (2014). *Climate Change 2014: Synthesis Report*. Contribution of Working Groups I, II and III to the Fifth Assessment Report of the Intergovernmental Panel on Climate Change [Core Writing Team, R.K. Pachauri and L.A. Meyer (eds.)]. IPCC, Geneva, Switzerland, 151 pp.

Irwin, W.P. & Barnes, I. (1980). Tectonic relations of carbon dioxide discharges and earthquakes. *Journal of Geophysical Research, 85*, 3115–3121.

Italiano, F., Kis, B.-M., Baciu, C., Ionescu, A., Harangi, S., & Palcsu, L. (2017). Geochemistry of dissolved gases from the Eastern Carpathians - Transylvanian Basin boundary. *Chemical Geology, 469*, 117–128.

Jančev, S., Pezdič, J., Szaran, J., & Halas, S. (1999). Characteristics of sulphate occurrences near Kosovrasti, Macedonia. *RMZ, 46*(3), 501–508.

This article is protected by copyright. All rights reserved.

Jenden, P.D., Titley, P.A., & Worden, R.H. (2015). Enrichment of nitrogen and ^{13}C of methane in natural gases from the Khuff Formation, Saudi Arabia, caused by thermochemical sulfate reduction. *Organic Geochemistry, 82*, 54–68.

Kerrick, D.M. (2001). Present and past nonanthropogenic CO_2 degassing from the solid earth. *Reviews of Geophysics, 39*, 565–585.

Kämpf, H., Brauer, K., Schumann, J., Hahne, K., & Strauch, G. (2013). CO_2 discharge in an active, non-volcanic continental rift area (Czech Republic): characterization ($\delta^{13}C$, $^3He/^4He$) and quantification of diffuse and vent CO_2 emissions. *Chemical Geology, 339*, 71–83.

Kerrick, D.M., & Caldeira, K. (1993). Metamorphic CO_2 degassing from orogenic belts. *Chemical Geology, 145*, 213-232.

Kerrick, D.M., McKibben, M.A., Seward, T.M., & Caldeira, K. (1995). Convective hydrothermal CO_2 emission from high heat flow region. *Chemical Geology, 121*, 285-293.

King, C.Y. (1986). Gas geochemistry applied to earthquake prediction: an overview. *Journal of Geophysical Research, 91*(B12) 12,269-12,281.

Kis, B.M., Ionescu, A., Cardellini, C., Harangi, S., Baciu, C., Caracausi, C., & Viveiros, F. (2017). Quantification of carbon dioxide emissions of Ciomadul, the youngest volcano of the Carpathian- Pannonian Region (Eastern- Central Europe, Romania). *Journal of Volcanology and Geothermermal Research, 341*, 119-130.

Kotevski, G. (1987). Hidrogeologija na mineralnite, termalnite i termomineralnite vodi na teritorijata na Socijalistichka Republika Makedonija (Hydrogeology of the mineral, thermal and thermomineral waters in the territory of the Socialist Republic of Macedonia). Samupravna praktika, Skopje, 352. (in Macedonian)

Lee, V.W., & Trifunac, M.D. (2017). Seismic hazard maps in Macedonia. *Soil Dynamics and Earthquake Engineering*, 100, 504-517.

Le Guern, F. (1982). Les debits de CO_2 et de SO_2 volcaniques dans l'atmosphere. *Bulletin of Volcanology, 45*(3), 197–202.

Lewicki, J., & Brantley, S.L. (2000). CO_2 degassing along the San Andreas Fault, Parkfield, California. *Geophysical Research Letters, 27*(1), 5-8.

Lewicki, J.L., Bergfeld, D., Cardellini, C., Chiodini, G., Granieri, D., Varley, N., & Werner, C. (2005). Comparative soil CO_2 flux measurements and geostatistical estimation methods on

This article is protected by copyright. All rights reserved.

Accepted Article

Masaya volcano, Nicaragua. *Bulletin of Volcanology, 68*, 76–90, doi: 10.1007/s00445-005-0423-9.

Lindhorst, K., Krastel, S., Reicherter, K., Stipp, M., Wagner, B., & Schwenk, T. (2015). Sedimentary and tectonic evolution of Lake Ohrid (Macedonia/Albania). *Basin Research, 27*, 84-101.

Markoski, B., Jovanovski, M., & Peshevski, I. (2019). *Duvalo - dry mofette, Kosel, Ohrid*. Geomap doo, Skopje. (in Macedonian with extended summary in English)

Marinković, G., Papić, P., Stojković, J., & Dragišić, V. (2012). Factors contributing to the formation of carbonated mineral water systems in Serbia. *Annales Geologiques de la Peninsule Balkanique, 73*, 117-124.

Machel, H.G. (2001). Bacterial and thermochemical sulfate reduction in diagenetic settings — old and new insights. *Sedimentary Geology, 140*, 143–175.

Martelli, M., Nuccio, P.M., Stuart, F.M., Burgess, R., Ellam, R.M., & Italiano, F. (2004). Helium-strontium isotope constraints on mantle evolution beneath the Roman Comagmatic Province, Italy, *Earth and Planetary Science Letters, 224*, 295–308.

Martelli, M., Rizzo, A.L., Renzulli, A., Ridolfi, F., Arienzo, I., & Rosciglione, A. (2014). Noble-gas signature of magmas from a heterogeneous mantle wedge: the case of Stromboli volcano (Aeolian Islands, Italy). *Chemical Geology, 368* (2014), 39–53.

Milkov, A.V., & Etiope, G. (2018). Revised genetic diagrams for natural gases based on a global dataset of >20,000 samples. *Organic Geochemistry, 125*, 109–120.

Minissale, A., Evans, W., Magro, G., & Vaselli, O. (1997). Multiple source components in gas manifestations from north-central Italy. *Chemical Geology, 142*, 175–192.

Mirčovski, V., Boev, B., Efremoski, Z., Šorša, A., & Dimov, D. (2015). Hydrochemical data for the ground waters in the Bitola's part of the Pelagonia Valley, Republic of Macedonia. *Geologica Macedonica, 29*(1), 15-24.

Mörner, N.K., & Etiope, G. (2002). Carbon degassing from the lithosphere. *Global Planetary Change, 33*, 185–203.

Molnár, K., Temovski, M., & Palcsu, L. (2021). First noble gas results from fluid inclusions of the Late Miocene-Pleistocene Macedonian volcanics, EGU General Assembly 2021, online, 19–30 Apr 2021, EGU21-9440, https://doi.org/10.5194/egusphere-egu21-9440.

This article is protected by copyright. All rights reserved.

Mougin, P., Lamoureux-Var, V., Bariteau, A., & Huc, A.Y. (2007). Thermodynamic of thermochemical sulphate reduction. *Journal of Petroleum Science and Engineering, 58*, 413–427.

Muirhead, J.D., Kattenhorn, S.A., Lee, H., Mana, S., Turrin, B.D., Fischer, T.P., Kianji, G., Dindi, E., & Stamps, D.S. (2016). Evolution of upper crustal faulting assisted by magmatic volatile release during early-stage continental rift development in the East African Rift. *Geosphere, 12*, 1670–1700.

Nisi, B., Vaselli, O., Marchev, P., & Tassi, F. (2013). Diffuse CO_2 Soil Flux Measurements at the Youngest Volcanic System in Bulgaria: The 12.2 Ma old Kozhuh Cryptodome. *Acta Vulcanologica, 25*(1–2), 169–177.

Ozima, M., & Podosek, F.A. (2002). *Noble Gas Geochemistry*. Cambridge University Press, 2nd, 286 p.

Parello, F., Allard, P., D'Alessandro, W., Federico, C., Jean-Baptiste, P., & Catani, O. (2000). Isotope geochemistry of Pantelleria volcanic fluids, Sicily Channel rift: A mantle volatile end-member for volcanism in southern Europe. *Earth and Planetary Science Letters, 180*, 325–339.

Pearce, J.M., Czernichowski-Lauriol, I., Lombardi, S., Brune, S., Nador, A., Baker, J., Pauwels, H., Hatziyannis, G., Beaubien, S., & Faber, E. (2004). A review of natural CO_2 accumulations in Europe as analogues for geological sequestration. *Geological Society London Special Pubblication, 233*, 29–41.

Peccerillo, A. (1999). Multiple mantle metasomatism in central-southern Italy: geochemical effects, timing and geodynamic implications. *Geology, 27*, 315–318.

Piperov, N.B., Kamensky, I.L, & Tolstikhn, I.N. (1994). Isotopes of the light noble gases in mineral waters in the eastern part of the Balkan peninsula, Bulgaria. *Geochimica et Cosmochimica Acta, 55*, 1889-1898.

Popovska-Vasilevska, S., & Armenski, S. (2016). Geothermal Potential of Macedonia and Its Utilization. In: *Mineral and Thermal Waters of Southeastern Europe*, Papić P. (ed.), Environmental Earth Sciences, Springer International Publishing Switzerland, doi: 10.1007/978-3-319-25379-4_8

Randazzo, P., Caracausi, A., Aiuppa, A., Cardellini, C., Chiodini, G., D'Alessandro, W., Li Vigni, L., Papic, P., Marinkovic, G., & Ionescu, A. (2021). Active degassing of deeply

This article is protected by copyright. All rights reserved.

Accepted Article

sourced fluids in central Europe: New evidences from a geochemical study in Serbia. *Geochemistry, Geophysics, Geosystems, 22*, e2021GC010017. https://doi.org/10.1029/2021GC010017

Reicherter K., Hoffmann N., Lindhorst K., Krastel S., Fernandez-Steeger T., Grutzner C., & Wiatr T. (2011): Active basins and neotectonics: morphotectonics of the Lake Ohrid basin (FYROM and Albania). *Zeitschrift der Deutschen Gesellschaft fur Geowissenschaften*, 162, 217–234.

Rizzo, A.L., Caracausi, A., Chavagnac, V., Nomikou, P., Polymenakou, P.N., Mandralakis, M., Kotoulas, G., Magoulas, A., Castillo, A., & Lampridou, D. (2016). Kolumbo submarine volcano (Greece): an active window into the Aegean subduction system. *Science Reports, 6*, 28013.

Robertson, A., & Shallo, M. (2000). Mesozoic-Tertiary tectonic evolution of Albania in its regional Eastern Mediterranean context, *Tectonophysics, 316*, 197–254.

Rogie, J.D., Kerrick, D.M., Chiodini, G., & Frondini, F. (2000). Flux measurements of nonvolcanic CO_2 emissions from some vents in central Italy. *Journal of Geophysical Research, 105*, 8435–8445.

Sano, Y., & Wakita, H. (1985). Geographical distribution of $^3He/^4He$ ratios in Japan: Implications for arc tectonics and incipient magmatism. *Journal of Geophysical Research, 90*, 8729–8741. doi: 10.1029/JB080i010p08729.

Sano, Y., & Marty, B. (1995). Origin of carbon in fumarolic gas from island arcs. *Chemical Geology, 119*, 265-274.

Schoell, M. (1983). Genetic characterization of natural gases. *America Association of Petroleum Geologists Bulletin*, 67, 2225−2238.

Šerif, A. (2001). Rudarstvoto vo Makedonija vo vreme na Osmanliskoto vladeenje (Mining in Macedonia during the Ottoman Rule), INI, Logos-A, Skopje. (in Macedonian)

Seward, T.M., & Kerrick, D.M. (1996). Hydrothermal CO_2 emission from the Taupo volcanic zone, New Zealand. *Earth and Planetary Science Letters, 139*, 105–113.

Shimizu, A., Sumino, H., Nagao, K., Notsu, K., & Mitropoulos, P. (2005). Variation in noble gas isotopic composition of gas samples from the Aegean arc, Greece. *Journal of Volcanology and Geothermermal Research, 140*, 321–339.

This article is protected by copyright. All rights reserved.

Sinclair, A.J. (1974). Selection of threshold values in geochemical data using probability graphs. *Journal of Geochemical Exploration, 3,* 129–149.

Schmid, S.M., Fügenschuh, B., Kounov, A., Maţenco, L., Nievergelt, P., Oberhänsli, R., Pleuger, J., Schefer, S., Schuster, R., Tomljenović, B., Ustaszewski, K., & van Hinsbergen, D.J.J. (2020). Tectonic units of the Alpine collision zone between Eastern Alps and western Turkey, *Gondwana Research, 78,* 308-374.

Tamburello, G., Pondrelli, S., Chiodini, G., & Rouwet, D. (2018). Global-scale control of extensional tectonic of CO_2 earth degassing. *Nature Communications, 9,* 4608.

Temovski, M., D'Alessandro, W., Ionescu, A., Li Vigni, L., Molnár, K., Palcsu, L., & Cardellini, C. (2020). Preliminary geochemical characterization of gas manifestations in North Macedonia. EGU2020-2763, EGU General Assembly 2020.

Tomkins, A.G. (2010). Windows of metamorphic sulfur liberation in the crust: Implications for gold deposit genesis. *Geochimica et Cosmochimica Acta,74,* 3246–59.

Trojanović, S. (1925). La Solfatare de Kosel. *Annales geologiques de la Peninsule Balkanique, 8*(1), 140-146.

Vaselli, O., Minissale, A., Tassi, F., Magro, G., Seghedi, I., Ioane, D., & Szakács, A. (2002). A geochemical traverse across the Eastern Carpathians (Romania): Constraints on the origin and evolution of the mineral water and gas discharges. *Chemical Geology, 182*, 637–654.

Viveiros, F., Cardellini, C., Ferreira, T., Caliro, S., Chiodini, G., & Silva, C. (2010). Soil CO_2 emissions at Furnas volcano, São Miguel Island, Azores archipelago: Volcano monitoring perspectives, geomorphologic studies and land use planning application. *Journal of Geophysics Research*, 115, B12208.

Viveiros, F., Chiodini, G., Cardellini, C., Caliro, S., Zanon, V., Silva, C., Rizzo, A.L., Hipòlito, A. & Moreno, L. (2020). Deep CO_2 emitted at Furnas do Enxofre geothermal area (Terceira Island, Azores archipelago). An approach for determining CO_2 sources and total emissions using carbon isotopic data. *Journal of Volcanology and Geothermal Research*, 401, 106968.

Wagner, B., Reicherter, B., Daut, G., Wessels, M., Matzinger, A., Schwalb, A., Spirkovski, Z., & Sanxhaku, M. (2008). The potential of Lake Ohrid for long-term palaeoenvironmental reconstructions. *Palaeogeography Palaeoclimatology Paleoecology, 259,* 341–356.

This article is protected by copyright. All rights reserved.

Accepted Article

Weinlich, F.H., (2014). Carbon dioxide controlled earthquake distribution pattern in the NW Bohemian swarm earthquake region, western Eger Rift, Czech Republic-gas migration in the crystalline basement. *Geofluids, 14*, 143–159.

Werner, C., Fischer, T. P., Aiuppa, A., Edmonds, M., Cardellini, C., Carn, S., Chiodini, G., Cottrell, E., Burton, M., Shinohara, H., & Allard, P. (2019). Carbon dioxide emissions from subaerial volcanic regions: Two decades in review. In: *Deep carbon past to present* (Chap. 8, pp. 188–236). Cambridge: Cambridge University Press.

World Meteorological Organization (2019). *The State of Greenhouse Gases in the Atmosphere Based on Global Observations through 2018*. WMO Greenhouse Gas Bulletin, n° 15.

Yanev, Y., Boev, B., Doglioni, C., Innocenti, F., Manetti, P., Pecskay, Z., Tonarini, S., & D'Orazio, M. (2008). Late Miocene to Pleistocene potassic volcanism in the Republic of Macedonia. *Mineralogy and Petrology, 94*, 45-60.

Yuçe, G., Fu, C.C., D'Alessandro, W., Gulbay, A.H., Lai, C.W., Bellomo, S., Yang, T.S., Italiano, F., & Walia, V. (2017). Geochemical characteristics of soil radon and carbon dioxide within the Dead Sea Fault and Karasu Fault in the Amik Basin (Hatay), Turkey. *Chemical Geology*, *469*, 129-146.

Zikov M. (1997): Temperatura na vozduhot, termički režim i klimatska podelba spored termičkiot režim vo Republika Makedonija (Air temperature, thermal regime and climatic division according to the thermal regime in Republic of Macedonia). In: Zikov M., Georgieva M., Andonovski T., Stojmilov A., Gramatikovski V., Bakeva V., Dimitrievski V. (eds): Vlijanieto na Sredozemnoto more vrz klimata na Republika Makedonija. Makedonska riznica, 39-73.

Accepted Article

This article is protected by copyright. All rights reserved.

Table 1 – Chemical and isotopic composition of the gases

Name	Date	N	E	He	H_2	O_2	N_2	CH_4	CO_2
		DD	DD	µmol/mol	µmol/mol	µmol/mol	µmol/mol	µmol/mol	µmol/mol
Duvalo	22.08.2019	41.16934	20.83719	70	38	128	17900	3250	966100
Duvalo 2	24.08.2019	41.16705	20.83868	29	1010	89000	381400	1370	508400
Duvalo 3	24.08.2019	41.16721	20.83924	< 3	108	161000	613300	463	213300
Duvalo 4	24.08.2019	41.16791	20.83914	< 3	756	189700	736100	11	63700
Duvalo	02.03.2020	41.16932	20.83721	62	< 3	19300	89800	2870	882600
Duvalo A	02.03.2020	41.16699	20.83865	56	< 3	26600	117900	2740	850800
Duvalo B	02.03.2020	41.16717	20.83918	51	< 3	19000	88800	3190	888400
Kosel 2	02.03.2020	41.17961	20.83500	5	10	205700	768200	3.7	2900
Velgoshti	02.03.2020	41.13395	20.83919	5	31	137800	841800	31	8700

Name	H_2S	C_2H_6	Ar	$\delta^{13}C(CO_2)$	$\delta^{13}C(CH_4)$	$\delta^{2}H(CH_4)$	R/R_A	error	He/Ne
	µmol/mol	µmol/mol	µmol/mol	‰ (vsV PDB)	‰ (vsV PDB)	‰ (vs VSMOW)			
Duvalo	5500	<10	79	-0.2	-34.4	-166	0.10	0.003	472
Duvalo 2	11	<10	n.a.	-0.1	-36.8	-158	n.a.	n.a.	n.a.
Duvalo 3	<10	<10	n.a.	2.7	n.a.	n.a.	n.a.	n.a.	n.a.
Duvalo 4	<10	<10	n.a.	-0.1	n.a.	n.a.	n.a.	n.a.	n.a.
Duvalo	5200	5.6	61	-0.8	-34.5	-180	0.10	0.004	2066
Duvalo A	3800	<10	n.a.	-0.8	-35.0	-175	n.a.	n.a.	n.a.
Duvalo B	4300	<10	n.a.	-0.8	-36.5	-169	n.a.	n.a.	n.a.
Kosel 2	<10	<10	9400	-13.7	n.a.	n.a.	n.a.	n.a.	n.a.
Velgoshti	<10	<10	10000	-0.8	n.a.	n.a.	n.a.	n.a.	n.a.

DD = decimal degrees; n.a. = not analysed

Table 2. Statistical parameters of CO_2 flux populations

Populations	Mean log CO_2 flux	σ log CO_2 flux	Proportion (%)	Mean CO_2 flux (g m^{-2} d^{-1})	95% confidence interval (g m^{-2} d^{-1})
A	1.32	0.54	30	45	35-62
B	2.71	0.46	59	897	746-1128
C	3.65	0.50	11	8382	6289-15161

This article is protected by copyright. All rights reserved.

Captions

Fig. 1 – Location of the study area; **a)** Ohrid region in relation to major geotectonic units of Republic of North Macedonia, adapted from Schmid et al. (2020); **b)** Elevation map of Ohrid Basin with geographic setting of Duvalo and Velogoshti sites; political border with Albania is shown in yellow line; **c)** panoramic photo of Duvalo area; **d)** dead hedgehog (red arrow) inside a hole with strong gas exhalation.

Fig. 2 - Geological settings of Duvalo site. Map compiled from geological data of Dumurdzanov & Ivanovski (1978) and Lindhorst et al. (2015). The geographical position of the sampling sites is evidenced by a star. The area investigated for CO_2 fluxes and mapped in Fig. 8 is evidenced by a box in the map on the right.

Fig. 3 – CO_2-N_2-O_2 ternary plot. The atmospheric air and air saturated water (ASW) compositions are also plotted.

Fig. 4 - Probability plot of the CO_2 fluxes from Duvalo area. The black lines represent the partitioned populations while the dashed red line represent the combination of the partitioned populations according to their relative proportions (see Table 2)

Fig. 5 - Binary plots of **a)** R/R_A vs. $^4He/^{20}Ne$ of the samples collected at Duvalo. The mixing lines between Atmosphere and a MORB-type Mantle and between Atmosphere and Crust are also plotted. Dashed lines represent mixing between atmosphere and end-members with different percentages of MORB-type mantle contribution (after Sano and Wakita, 1985). Three other mantle end-members are also reported: SCLM (Subcrustal Litospheric Mantle – Gautheron and Moreira, 2002); SMX (Stromboli Mantle Xenoliths – Martelli et al., 2014); RMP (Roman Magmatic Province – Martelli et al., 2004) **b)** $CO_2/^3He$ vs. $\delta^{13}C$-CO_2. The compositions for Sediments, MORB-like Mantle and Limestones end-members are: $\delta^{13}C$-CO_2 = -30 ‰, -6.5 ‰ and 0 ‰ and $CO_2/^3He = 1\times10^{13}$, 1.5×10^9 and 1×10^{13}, respectively (after Sano and Marty, 1995). Percent of mantle contribution is shown along the mixing line between mantle and respectively limestones and sediments. SCLM from Bräuer et al. (2016) and SMX from Martelli et al. (2014) and Gennaro et al. (2017). Samples from other sites of the Republic of North Macedonia

This article is protected by copyright. All rights reserved.

Accepted Article

(Temovski et al., 2020) and of the nearby northern Greece region (Daskalopoulou et al., 2018) are plotted for comparison.

Fig. 6 - $\delta^{13}C\text{-}CH_4$ vs. $\delta^{2}H\text{-}CH_4$ **a)** and $\delta^{13}C\text{-}CH_4$ vs. $C_1/(C_2+C_3)$ **b)** genetic diagrams (Milkov and Etiope, 2018). CR = CO_2 reduction; F = methyl-type fermentation.

Fig. 7 – H_2S, CH_4 and He vs. CO_2 binary plot. The dashed lines represent the mixing between atmospheric air and the deep geogenic gas.

Fig. 8. - a) map of the CO_2 flux; white dots refer to measured sites; red lines are inferred diffuse degassing structures which follow the directions of the tectonic lineaments defined by Dumurdzanov & Ivanovski (1978); **b)** experimental variogram and variogram model.

This article is protected by copyright. All rights reserved.

Accepted Article

Appendix

Table A1. CO_2 flux measurements

Point	Coordinates		CO_2 flux		Point	Coordinates		CO_2 flux
	E	N	g m^{-2} d^{-1}			E	N	g m^{-2} d^{-1}
PA1	486286	4557735	462		PA56	486349	4557570	736
PA2	486275	4557724	158		PA57	486343	4557567	34,612
PA3	486267	4557713	179		PA58	486336	4557563	143
PA4	486254	4557705	5,680		PA59	486329	4557557	664
PA5	486242	4557696	698		PA60	486321	4557553	4,706
PA6	486232	4557688	204		PA61	486318	4557545	273
PA7	486248	4557660	137		PA62	486329	4557548	1,349
PA8	486261	4557665	484		PA63	486338	4557552	1,903
PA9	486273	4557672	894		PA64	486344	4557557	3,412
PA10	486285	4557681	311		PA65	486349	4557562	1,063
PA11	486297	4557687	501		PA66	486355	4557567	1,823
PA12	486308	4557696	142		PA67	486362	4557561	17,139
PA13	486317	4557661	28.7		PA68	486354	4557555	12,996
PA14	486306	4557650	3,263		PA69	486345	4557548	59,259
PA15	486297	4557643	491		PA70	486337	4557542	1,815
PA16	486287	4557637	240		PA71	486339	4557535	300
PA17	486279	4557634	1687		PA72	486347	4557522	282
PA18	486268	4557632	198		PA73	486355	4557516	1,250
PA19	486260	4557629	301		PA74	486362	4557507	5,140
PA20	486252	4557622	41.8		PA75	486359	4557500	1.34
PA21	486239	4557618	30.3		PA76	486351	4557508	2,989
PA22	486261	4557605	13.6		PA77	486342	4557511	211
PA23	486274	4557609	32.4		PA78	486329	4557509	249
PA24	486286	4557613	99.6		PA79	486316	4557508	488
PA25	486297	4557618	61.5		PA80	486302	4557507	7.02
PA26	486308	4557622	4,158		PA81	486307	4557494	11.9
PA27	486314	4557625	798		PA82	486319	4557495	5,746
PA28	486328	4557637	1,631		PA83	486333	4557497	1,061
PA29	486331	4557642	46.5		PA84	486345	4557499	863
PA30	486343	4557614	129		PA85	486348	4557464	1,151
PA31	486328	4557611	189		PA86	486335	4557463	3,790
PA32	486319	4557607	587		PA87	486321	4557459	17.2
PA33	486308	4557602	1,595		PA88	486330	4557448	15.4
PA34	486299	4557597	167		PA89	486342	4557454	950
PA35	486289	4557594	75.7		PA90	486350	4557456	622
PA36	486276	4557589	479		PA91	486363	4557456	7.96
PA37	486265	4557586	48.2		PA92	486359	4557448	36.6
PA38	486254	4557586	66.6		PA93	486359	4557440	671
PA39	486242	4557583	24.3		PA94	486363	4557438	204
PA40	486264	4557576	60.1		PA95	486367	4557433	1,401
PA41	486282	4557584	393		PA96	486372	4557432	120
PA42	486293	4557589	100		PA97	486381	4557430	2,089
PA43	486304	4557593	353		PA98	486396	4557429	1,981
PA44	486314	4557597	833		PA99	486390	4557427	1,776
PA45	486329	4557600	2,592		PA100	486393	4557423	4,273
PA46	486338	4557603	378		PA101	486406	4557411	535
PA47	486351	4557609	125		PA102	486415	4557409	823
PA48	486359	4557592	60.5		PA103	486428	4557406	398
PA49	486350	4557586	4.93		PA104	486434	4557417	1,688
PA50	486344	4557578	864		PA105	486443	4557414	1,438
PA51	486336	4557574	6,401		PA106	486452	4557419	476
PA52	486329	4557570	6,127		PA107	486444	4557403	490
PA53	486321	4557566	499		PA108	486458	4557403	612
PA54	486312	4557561	6,409		PA109	486473	4557397	407
PA55	486302	4557557	975		PA110	486473	4557409	1,280

This article is protected by copyright. All rights reserved.

Table A1. *(Continued)*

Point	Coordinates		CO_2 flux		Point	Coordinates		CO_2 flux
	E	N	g m^{-2} d^{-1}			E	N	g m^{-2} d^{-1}
PA111	486473	4557416	1,074		PA167	486445	4557380	678
PA112	486474	4557426	34.3		PA168	486470	4557363	15.3
PA113	486494	4557417	95.3		PA169	486474	4557344	54.1
PA114	486497	4557422	4.24		PA170	486510	4557358	99.7
PA115	486505	4557422	2.23		PA171	486548	4557360	38.2
PA116	486513	4557421	12.4		PA172	486546	4557380	61.2
PA117	486514	4557412	3,070		PA173	486525	4557383	48.9
PA118	486507	4557416	141		PA174	486499	4557382	19.0
PA119	486500	4557413	2,659		PA175	486447	4557348	19.1
PA120	486505	4557409	2,821		PA176	486418	4557344	4.71
PA121	486493	4557410	2,423		PA177	486417	4557362	18.4
PA122	486419	4557326	135		PA178	486385	4557373	14.2
PA123	486414	4557319	616		PA179	486346	4557377	8.59
PA124	486432	4557307	560		PA180	486309	4557381	13.8
PA125	486439	4557304	959		PB1	486289	4557711	418
PA126	486444	4557297	1,050		PB2	486278	4557705	859
PA127	486451	4557290	1,023		PB3	486269	4557697	592
PA128	486461	4557283	646		PB4	486258	4557691	136
PA129	486468	4557279	607		PB5	486247	4557680	474
PA130	486472	4557269	5,848		PB6	486254	4557645	51.3
PA131	486479	4557261	1,642		PB7	486262	4557651	305
PA132	486483	4557253	14,025		PB8	486275	4557654	745
PA133	486489	4557250	4,194		PB9	486285	4557661	55.0
PA134	486500	4557240	249		PB10	486298	4557667	421
PA135	486506	4557246	2,510		PB11	486311	4557675	163
PA136	486511	4557251	1,198		PB12	486324	4557644	1,775
PA137	486509	4557258	384		PB13	486315	4557638	3,372
PA138	486502	4557258	552		PB14	486308	4557633	816
PA139	486490	4557255	1,359		PB15	486297	4557626	192
PA140	486502	4557251	30,806		PB16	486284	4557622	147
PA141	486493	4557265	2,203		PB17	486270	4557620	133
PA142	486486	4557270	9,611		PB18	486260	4557615	23.3
PA143	486479	4557269	20.3		PB19	486249	4557615	7.58
PA144	486485	4557259	632		PB20	486329	4557623	216
PA145	486469	4557288	2,024		PB21	486316	4557617	1,474
PA146	486476	4557280	584		PB22	486309	4557613	584
PA147	486470	4557308	940		PB23	486299	4557608	131
PA148	486474	4557316	1,369		PB24	486289	4557605	275
PA149	486478	4557323	395		PB25	486279	4557601	15.8
PA150	486483	4557330	383		PB26	486266	4557598	22.3
PA151	486491	4557336	943		PB27	486254	4557598	5.91
PA152	486504	4557323	1,375		PB28	486269	4557563	53.7
PA153	486510	4557329	15,000		PB29	486281	4557568	761
PA154	486520	4557347	8,363		PB30	486291	4557575	29.5
PA155	486515	4557339	8,945		PB31	486304	4557579	53.6
PA156	486473	4557326	2,790		PB32	486319	4557583	158
PA157	486466	4557317	8,036		PB33	486333	4557586	2,262
PA158	486455	4557306	2,192		PB34	486345	4557592	410
PA159	486282	4557554	14.4		PB35	486352	4557598	1,011
PA160	486262	4557514	7.68		PB36	486360	4557604	239
PA161	486288	4557516	22.9		PB37	486361	4557582	20.7
PA162	486289	4557485	3.65		PB38	486356	4557581	38.7
PA163	486293	4557439	5.31		PB39	486346	4557573	6,712
PA164	486327	4557417	10.7		PB40	486354	4557574	1,157
PA165	486362	4557397	15.0		PB41	486363	4557575	10.0
PA166	486401	4557387	5.19		PB42	486359	4557569	535

This article is protected by copyright. All rights reserved.

Table A1. *(Continued)*

Point	Coordinates		CO_2 flux		Point	Coordinates		CO_2 flux
	E	N	g m^{-2} d^{-1}			E	N	g m^{-2} d^{-1}
PB43	486367	4557569	3,909		PB93	486486	4557395	324
PB44	486370	4557563	1,617		PB94	486495	4557396	282
PB45	486368	4557557	57.6		PB95	486502	4557396	1,926
PB46	486362	4557554	29.4		PB96	486511	4557398	453
PB47	486365	4557542	57.2		PB97	486518	4557396	88.2
PB48	486373	4557542	13.1		PB98	486497	4557404	1,572
PB49	486375	4557551	656		PB99	486508	4557406	587
PB50	486351	4557544	46.3		PB100	486521	4557410	893
PB51	486320	4557558	149		PB101	486416	4557310	262
PB52	486314	4557553	145		PB102	486422	4557316	245
PB53	486306	4557548	43.9		PB103	486427	4557322	176
PB54	486316	4557534	3.97		PB104	486427	4557331	151
PB55	486326	4557537	198		PB105	486434	4557321	91.1
PB56	486334	4557531	67.8		PB106	486431	4557316	117
PB57	486321	4557528	150		PB107	486427	4557311	389
PB58	486309	4557524	131		PB108	486421	4557305	125
PB59	486314	4557517	93.1		PB109	486443	4557322	14.0
PB60	486328	4557519	201		PB110	486450	4557316	27.1
PB61	486341	4557519	107		PB111	486443	4557310	207
PB62	486346	4557490	1,717		PB112	486427	4557301	11.4
PB63	486335	4557487	737		PB113	486435	4557297	293
PB64	486319	4557483	40.9		PB114	486438	4557289	27.8
PB65	486306	4557479	8.11		PB115	486450	4557281	4.11
PB66	486345	4557476	437		PB116	486460	4557274	25.0
PB67	486329	4557474	897		PB117	486465	4557266	20.8
PB68	486316	4557469	764		PB118	486468	4557258	64.3
PB69	486343	4557445	16.5		PB119	486474	4557250	221
PB70	486333	4557440	2,141		PB120	486481	4557244	600
PB71	486353	4557450	652		PB121	486490	4557240	1,692
PB72	486342	4557431	10.0		PB122	486458	4557297	153
PB73	486353	4557440	13.7		PB123	486463	4557302	883
PB74	486358	4557434	2.68		PB124	486477	4557292	726
PB75	486357	4557425	13.2		PB125	486466	4557295	2,917
PB76	486363	4557423	2.36		PB126	486473	4557300	898
PB77	486371	4557420	1.58		PB127	486479	4557309	767
PB78	486379	4557421	2.36		PB128	486482	4557315	565
PB79	486386	4557424	1,270		PB129	486488	4557324	981
PB80	486388	4557433	59.7		PB130	486499	4557332	685
PB81	486395	4557419	1,017		PB131	486504	4557341	947
PB82	486402	4557430	588		PB132	486508	4557348	149
PB83	486397	4557412	544		PB133	486495	4557344	97.5
PB84	486404	4557400	31.4		PB134	486484	4557340	34.1
PB85	486419	4557395	57.9		PB135	486478	4557336	43.7
PB86	486438	4557394	77.9		PB136	486471	4557330	190
PB87	486457	4557393	2,284		PB137	486462	4557323	15.0
PB88	486463	4557419	676		PB138	486407	4557329	123
PB89	486463	4557412	84.5		PB139	486396	4557339	50.0
PB90	486486	4557424	871		PB140	486383	4557347	67.4
PB91	486486	4557416	575		PB141	486371	4557358	125
PB92	486485	4557406	306					

Coordinates UTM zone 34 T. All measurements have been made on the 23rd and 24th August 2019, except at sites from PA 159 to PA 180 made on the 2nd of March 2020. Temperature at 50 cm depth has been measured only at the following sites: PA57 (17.7 °C), PA69 (18.1 °C), PA117 (18.2 °C), PA153 (18.5 °C) and PA157 (17.2 °C).

This article is protected by copyright. All rights reserved.

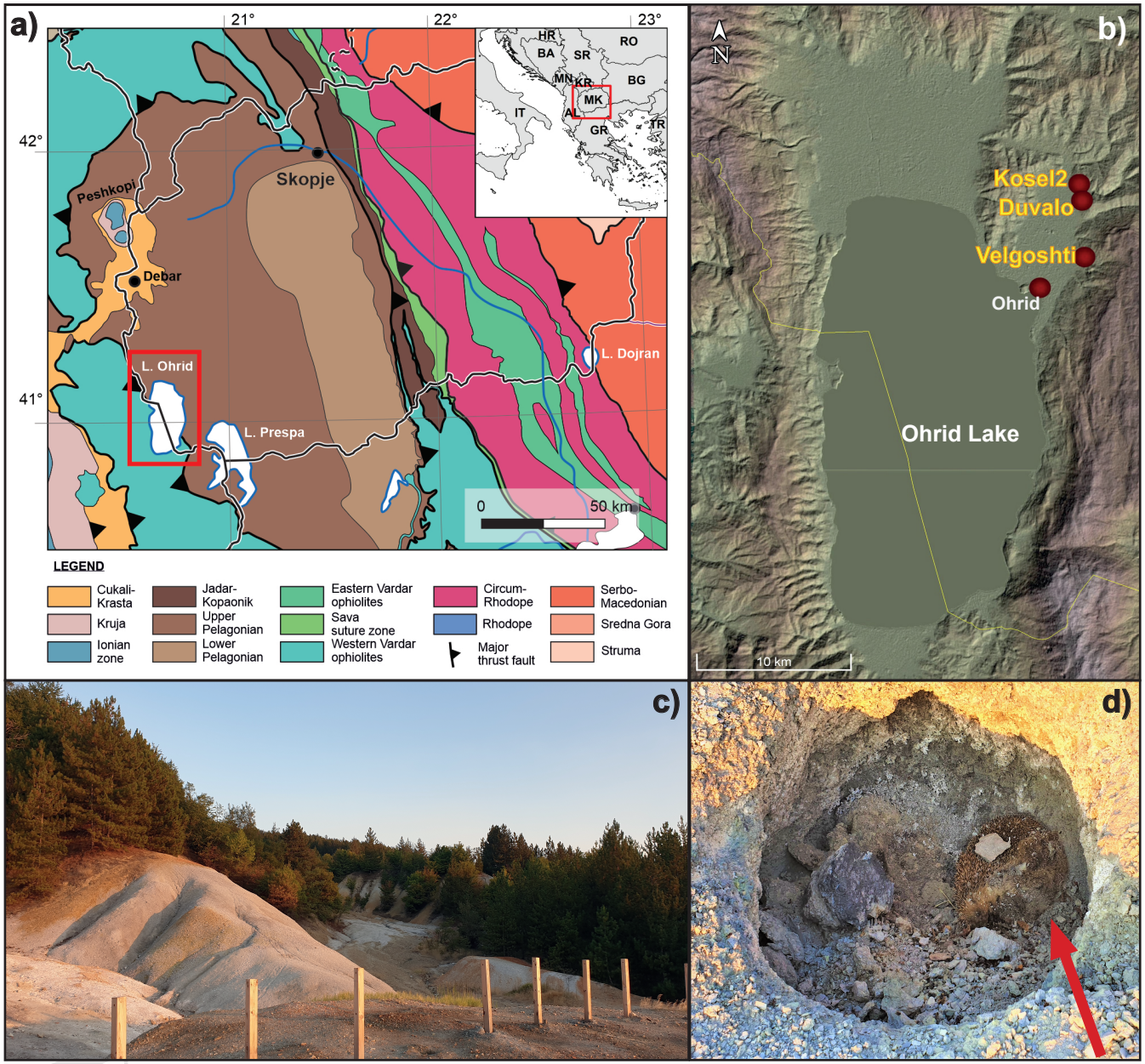

This article is protected by copyright. All rights reserved.

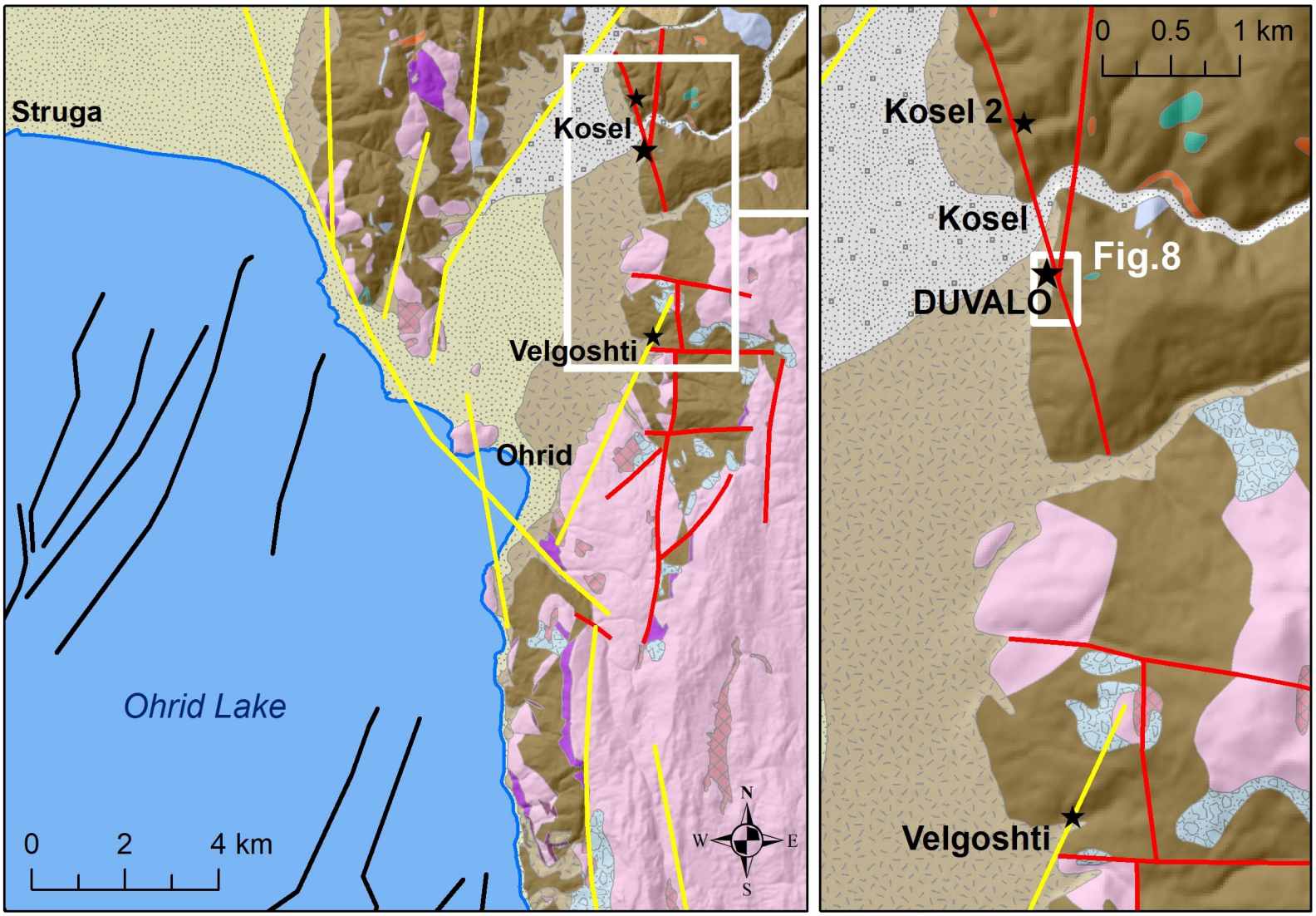

Legend

- Alluvial deposits (Q)
- Lacustrine deposits (Q)
- Proluvial deposits (Q)
- Slope breccia (Q)
- Terra rossa (Q)
- Fluvial and lacustrine deposits (N)
- Serpetinite (J)
- Diabase (J)
- Granitoids (J)
- Limestone and dolomite (T)
- Clastic sediments (T)
- Carbonate schist and marble (Pz)
- Quartz-sericite-graphite schist (Pz)
- Fault (Dumurdzanov & Ivanovski 1978)
- Fault (Lindhorst et al. 2015)
- Active fault in Ohrid Lake sediments (Lindhorst et al. 2015)

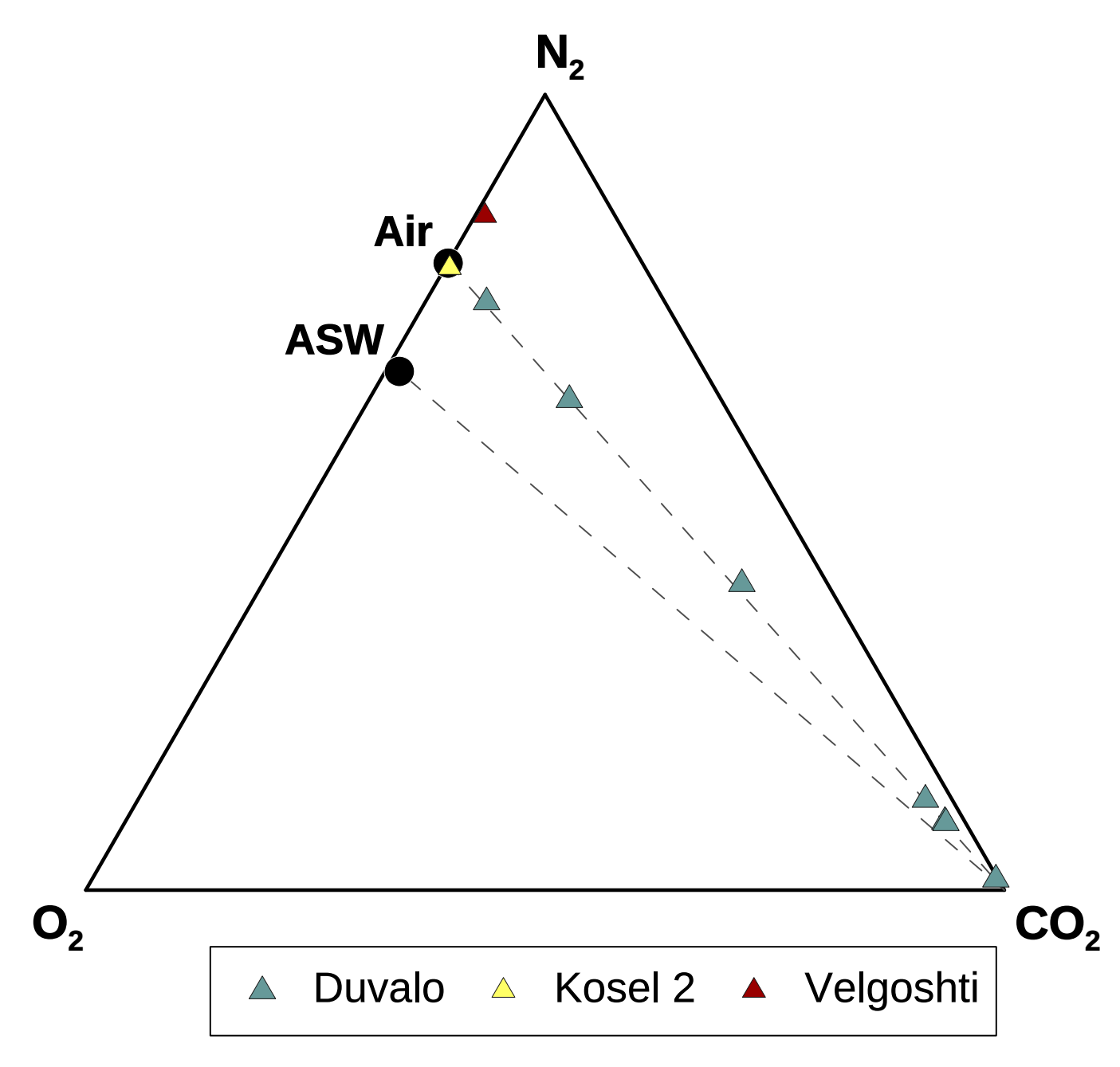
N_2
Air
ASW
O_2
CO_2
Duvalo
Kosel 2
Velgoshti

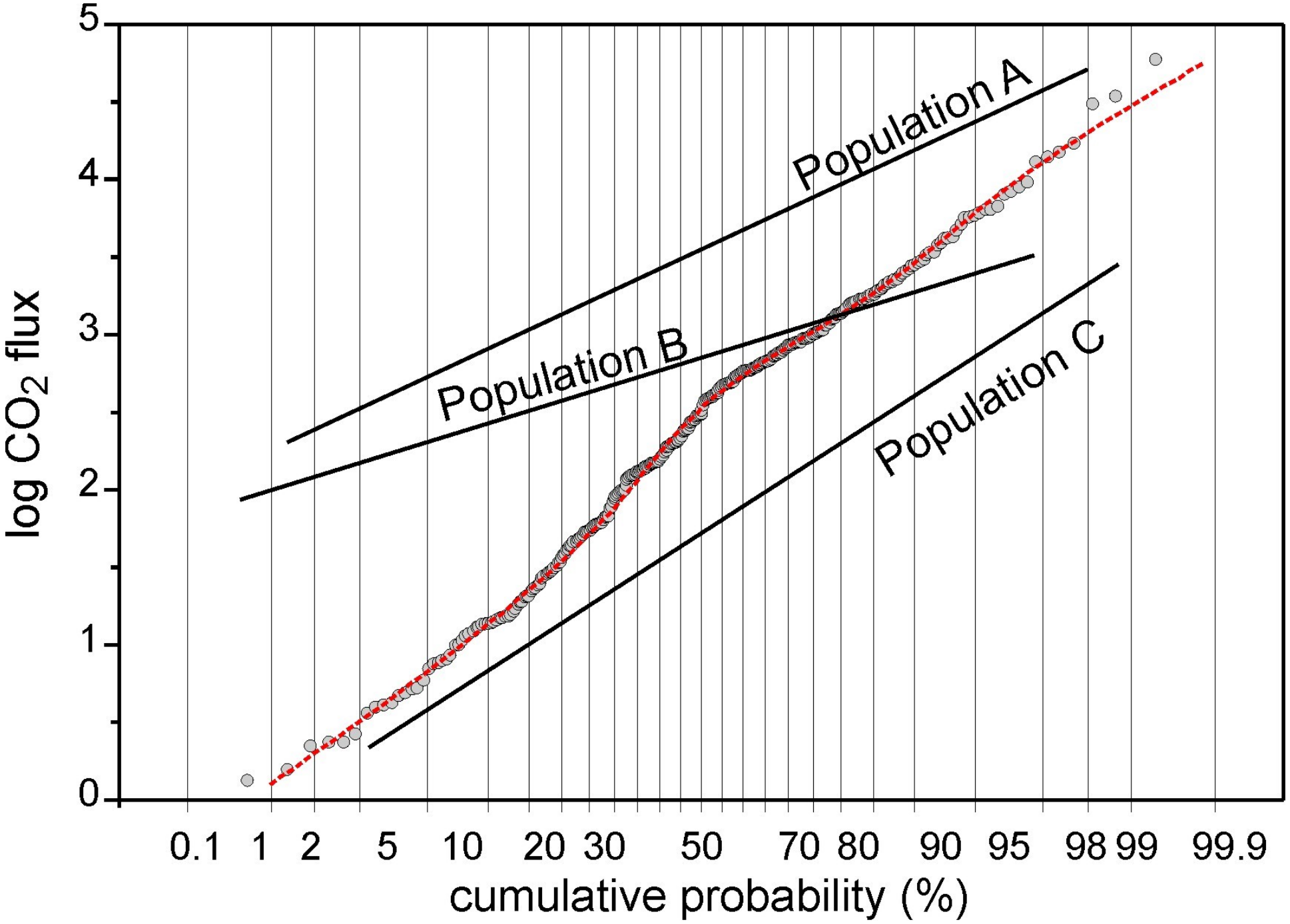
log CO_2 flux
0
1
2
3
4
5
0.1
1
2
5
10
20
30
50
70
80
90
95
98
99
99.9
cumulative probability (%)
Population A
Population B
Population C

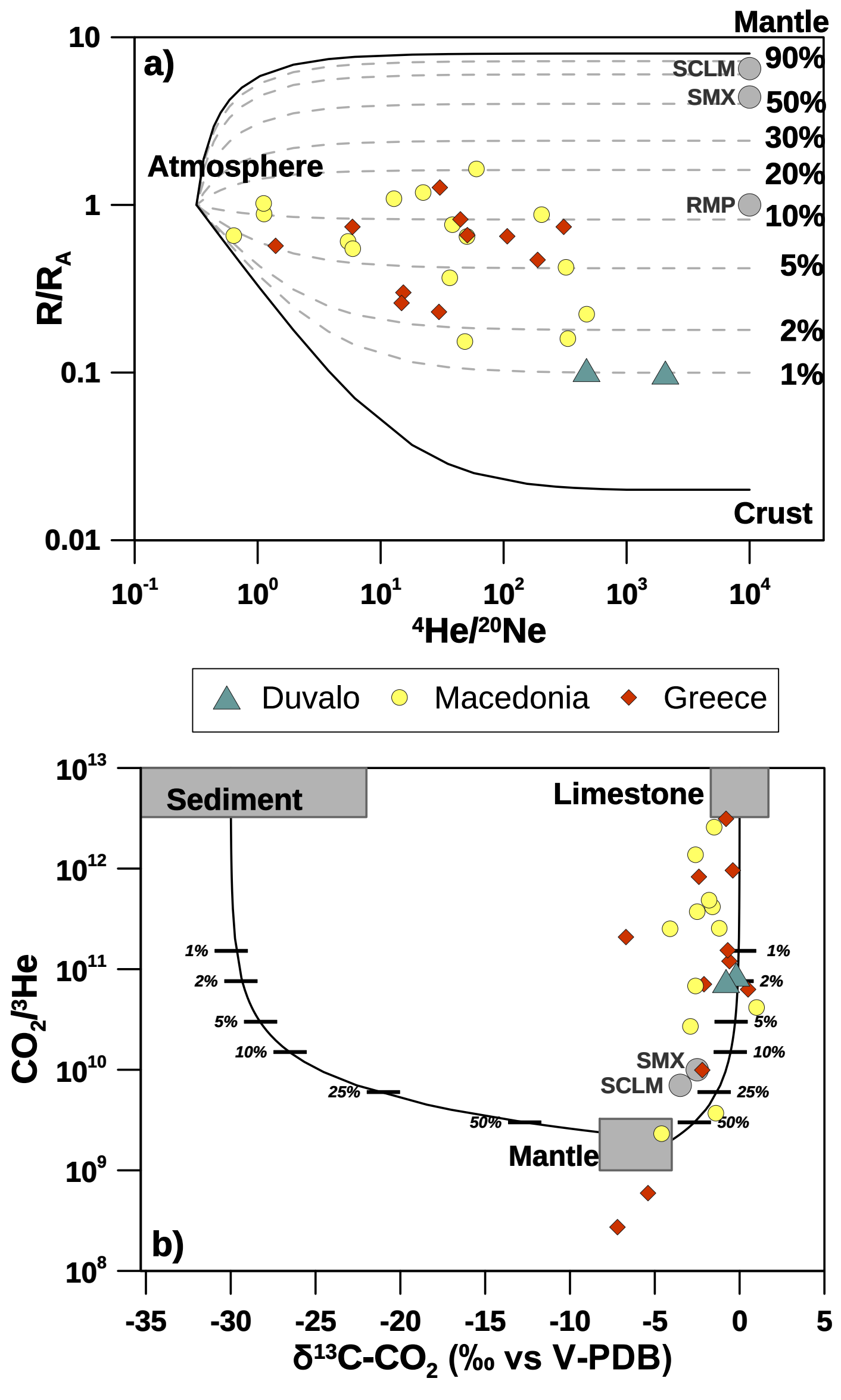
a)
Mantle
Crust
Atmosphere
SCLM
SMX
RMP
90%
50%
30%
20%
10%
5%
2%
1%
R/R_A
10
1
0.1
0.01
10^-1
10^0
10^1
10^2
10^3
10^4
4He/20Ne
Duvalo
Macedonia
Greece
b)
Sediment
Limestone
Mantle
SMX
SCLM
1%
2%
5%
10%
25%
50%
CO2/3He
10^13
10^12
10^11
10^10
10^9
10^8
-35
-30
-25
-20
-15
-10
-5
0
5
δ13C-CO2 (‰ vs V-PDB)

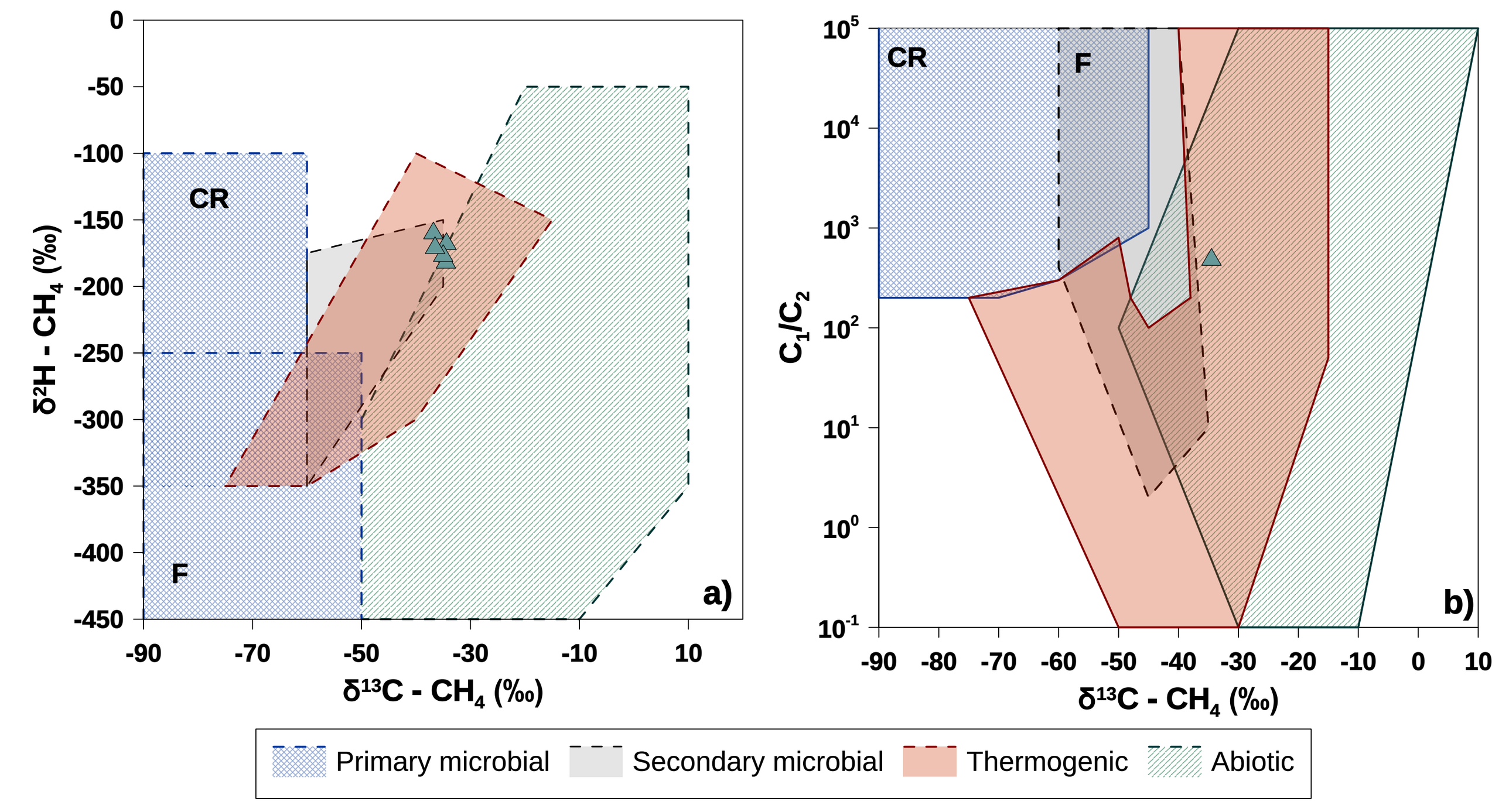
0
-50
-100
-150
-200
-250
-300
-350
-400
-450
δ²H - CH4 (‰)
CR
F
a)
-90
-70
-50
-30
-10
10
δ13C - CH4 (‰)
10^5
10^4
10^3
10^2
10^1
10^0
10^-1
C1/C2
CR
F
b)
-90
-80
-70
-60
-50
-40
-30
-20
-10
0
10
δ13C - CH4 (‰)
Primary microbial
Secondary microbial
Thermogenic
Abiotic

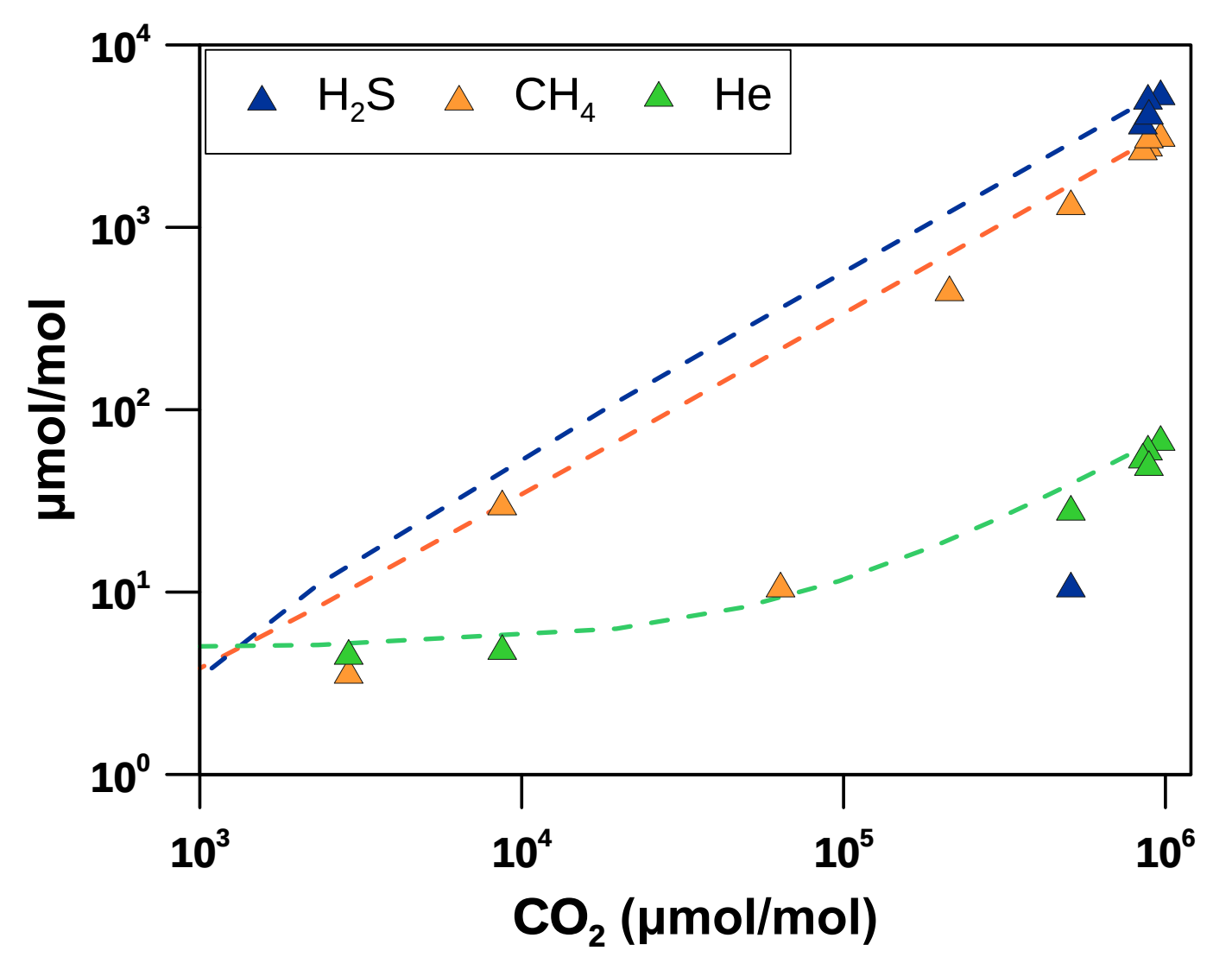
H2S
CH4
He
10^4
10^3
10^2
10^1
10^0
µmol/mol
10^3
10^4
10^5
10^6
CO2 (µmol/mol)

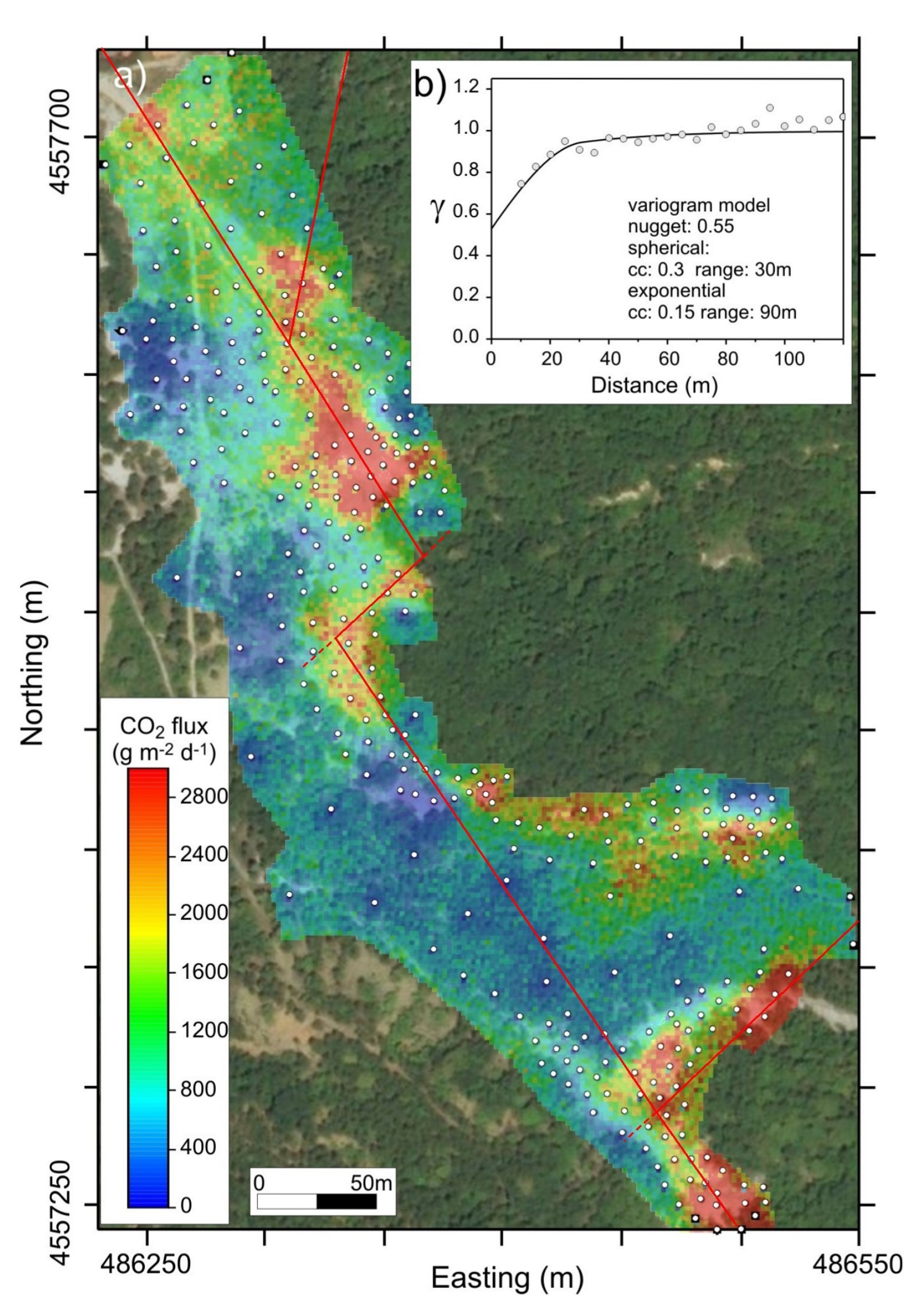
a)
b)
1.2
1.0
0.8
γ 0.6
0.4
0.2
0.0
0
20
40
60
80
100
Distance (m)
variogram model
nugget: 0.55
spherical:
cc: 0.3 range: 30m
exponential
cc: 0.15 range: 90m
CO2 flux
(g m-2 d-1)
2800
2400
2000
1600
1200
800
400
0
0
50m
4557700
4557250
Northing (m)
486250
486550
Easting (m)